CONTRACT NASW 4617 -- FINAL REPORT

Detection of Dust Impacts by the Voyager Planetary Radio Astronomy Experiment

Dr. David R. Evans
Radiophysics, Inc.
5475 Western Avenue
Boulder, CO 80301
Telephone: (303) 447-9524

ABSTRACT

The PRA instrument detected large numbers of dust particles during the Voyager 2 encounter with Neptune. We here analyse the signatures of these impacts in some detail. The major conclusions are:-

1. PRA detects impacts from all over the spacecraft body, not just the PRA antennas;

2. The signatures of individual impacts last substantially longer than was expected from complementary PWS data acquired by another Voyager experiment;

3. The signatures of individual impacts demonstrate very rapid fluctuatiions in signal strength, so fast that the data are limited by the speed of response of the instrument;

4. The PRA detects events at a rate consistently lower than does the Plasma Wave subsystem;

5. Even so, the impact rate is so great near the inbound crossing of the ring plane that no reliable estimate of impact rate can be made for this period;

6. The data are consistent with the presence of electrons accelerated by ions within an expanding plasma cloud from the point of impact.

An ancillary conclusion is that the anomalous appearance of data acquired at 900 kHz appears to be due to an error in processing the PRA data prior to their delivery to the experiment's Principal Investigator, rather than due to overload of the PRA instrument.

1. INTRODUCTION

The Voyager 2 encounter with Neptune presented the scientific community with a large number of unparalled opportunities for performing new science. Amongst these was the detection of dust impacts occuring on the spaceraft body or the antennas of the Planetary Radio Astronomy ("PRA") experiment using the PRA instrument in a "high rate" mode. The examination of the signatures caused by such impacts is the subject of this report.

2. BACKGROUND

An unexpected series of observations were made by the Voyager Planetary Radio Astronomy and Plasma Wave Subsystem ("PWS") experiments during the Voyager 2 encounter with Saturn. It became clear during analysis of the data from this encounter that both experiments were capable of detecting and recording impacts of micron sized dust particles against the body of the spacecraft as it passed through the region of the planet's ring plane (Scarf *et al.*, 1982; Warwick *et al.*, 1982). Similar measurements were made also at Uranus (Gurnett *et al.*, 1986; Warwick *et al.*, 1986), and it was expected that dust impacts would again be observed during the Voyager 2 Neptune encounter.

3. INSTRUMENTATION

For the encounters with Saturn and Uranus, the PRA instrument was operating in a low data rate scanning mode at the times that the dust impacts occured. In this mode, individual impacts are unresolved, and many, many impacts remain undetected. Spacecraft resources were too limited for the PRA team to be successful in obtaining data in any more effective mode, however. This situation was slightly different for the Neptune encounter and, in addition to the usual low rate scanning data, several periods of high rate PRA data were also acquired. High rate PRA data are acquired in units of "frames", each 48 seconds in duration. In its high rate mode, the PRA operates very differently from its operation in any of its more common low rate modes. In a canonical 48 second frame, the following series of events occurs:

1. The bandwidth of the instument channels becomes 200 kHz;

2. A pair of frequency channels whose central frequencies are separated by 307.2 kHz are designated;

3. For a period of 24 seconds, each channel of the selected pair is sampled; each sample is made simultaneously in the two channels, but the resulting measurements are recorded sequentially in the data stream;

4. Each datum so recorded comprises an eight bit data number which can then be converted to a calibrated power level on the ground;

5. Instead of passing through the usual long duration integrating filters in the PRA, each the signal passes through a simple RC circuit with a time constant of 100 microseconds before being digitised and stored; no signal integration occurs;

6. The channels are sampled simultaneously at intervals of 138.8888 microseconds;

7. After 400 pairs of samples have been made, there is a 4.444 millisecond data gap, after which sampling begins once more;

8. After 24 seconds have elapsed, a second frequency pair spaced by 307.2 kHz is chosen and the sampling recommences;

9. At all times, the senses of circular polarisation of the two samples that comprise a pair are opposite.

A pictorial representation of the format of high rates frames acquired during Neptune encounter is given in Figure 1. This configuration remained unchanged throughout the encounter period.

3.1. TERMINOLOGY

The PRA high rate signals follow a path through the spacecraft Flight Data System ("FDS") that is usually reserved for the imaging subsystem, and much of the terminology used in reference to the high rate data reflects this heritage. We speak of 48 second frames; each frame comprises 800 "lines"; the duration of a line is 55.555 milliseconds. The imaging subsystem has a 4.444 millisecond flyback time at the end of each line; a similar data gap occurs in the PRA data. Thus, although individual lines contain only 55.555 milliseconds of data, there is exactly 60.000 milliseconds between the start of one line and the start of the immediately succeeding one.

Each line contains 800 data, arranged as 400 simultaneously acquired data pairs. Within a data pair we refer to channel 1 (the higher frequency channel of the pair) and channel 2 (the lower frequency channel). Each frame is identified by a unique number, which represents (in an encoded way) the time of acquisition of the frame. The spacecraft FDS clock increments by 0.01 every 48 seconds, in a mod 60 manner, so that an increment of unity in the spacecraft clock represents a period of 48 minutes. Each frame is marked by the reading on the spacecraft clock at the time of the beginning of the frame. The reading on the spacecraft clock is termed the "FDS count". The corresponding time (in Universal Coordinated Time) is termed the Spacecraft Event Time ("SCET").

4. COORDINATE SYSTEMS

It is necessary to define three relevant coordinate systems carefully. The first of these is used to express spacecraft position with respect to Neptune, the second expresses the spacecraft velocity vector and the third expresses spacecraft orientation.

4.1. POSITION

The Voyager mission uses a neptunian rotation period of 16.11 hours, which was derived from the periodic modulation of radio emissions (Warwick *et al.*, 1989), with a subspacecraft longitude at closest approach defined to be 168°. (Longitude

increases to the west on the planet's surface; that is, the subspacecraft longitude of a stationary spacecraft increases monotonically with time, except at 360°.) We define a radius/latitude/longitude coordinate system then in which the radial distance of the spacecraft, r, is measured in units of the equatorial neptunian radius ($1R_N = 24,760$ km) from the planetary centre, and the two angles are the sub-spacecraft latitude and longitude as defined by the Voyager project. Coordinates in this system will be given as a triad: R(a, b, c), where a is the distance in radii, b is the latitude in degrees, and c is the (westward) longitude in degrees.

4.2. VELOCITY

The second coordinate system is simply a time derivative cartesian equivalent of the first. As the velocity of the spacecraft is small compared to the neptunian radius, values in this system are given in kilometres per second. It will be written as X(a, b, c) where a, b, c are the velocity components in the directions of the x, y, and z axes respectively.

4.3. ORIENTATION

For spacecraft orientation we adopt a coordinate system that is physically meaningful for the PRA experiment. Two angles are important in this system; these angles are denoted θ and ϕ. We first define a right handed cartesian system with the x and y axes running along the two (orthogonal) PRA antennas and the z axis along the (orthogonal) direction opposite to that of the magnetometre boom. The origin of the system is the point near the base of the antennas where these three axes meet. In this system, θ is the colatitude of a vector to a point with respect to the z axis and ϕ is the azimuth of the vector relative to the x axis. The orientation of the spacecraft is completely defined by the two values θ and ϕ for the line joining the origin of the coordinate system to the centre of the planet. The orientation is given by Λ(a, b) where a is θ in degrees and b is ϕ in degrees.

5. THE FRAMES

During the period of closest approach to Neptune, the encounter timeline was arranged so that the spacecraft would return five

high rate frames, acquired in four distinct locations (two of the frames were returned as a contiguous pair near to the expected time of the first ring plane crossing). The raw, uncalibrated data returned during these frames are shown as Figures 2 through 6; calibrated versions of these frames are given in Figures 7 through 11. Table 1 gives pertinent coordinate information for each frame. Each of the frames shows one or more dust impacts.

We will summarise the overall data on a frame by frame basis.

5.1. Frame 11386.08 (Figure 2; Figure 7)

This frame was acquired at SCET 1989:237:0:36:47. At this time the spacecraft was located at position R(9.52, -17.88, 6.35) and travelling with a velocity X(-16.18, -0.13, 8.69). Its orientation was Λ(51.32, 63.45).

A single dust impact appears on this frame, approximately six seconds before the end of the frame. That any impacts at all are present in this frame (acquired eight and a half radii above the planet's cloudtops) is a testament to the extreme dustiness of the neptunian environment. If no other frames showed dust impacts, it is almost certain that the single event on this frame would have been either ignored or ascribed to a single broadband radio discharge event such as is commonly associated with lightning. A comparison of Figure 12, which shows a detail of this single event, with detailed plots of events which are indubitably dust impacts (see below) demonstrates, however, that this lone event is indeed the signature of a dust impact impacting the spacecraft or antennas.

5.2. Frames 11388.56 (Figure 3; Figure 8) and 11388.57 (Figure 4; Figure 9)

These contiguous frames were acquired over a period of forty eight seconds on either side of SCET 1989:237:2:51:59, near inbound ringplane crossing. At this time, the spacecraft was located at position R(3.50, -0.38, 60.61) and travelling with a velocity X(-10.39, 14.79, 9.52). Its orientation was Λ(69.28, 62.70)). A large number of impacts occur on these frames.

5.3. Frame 11390.28 (Figure 5; Figure 10)

This frame was acquired near the spacecraft's closest approach to the planet, at position R(1.29, 61.15, 244.60). Even though the spacecraft is far from the ringplane, several impacts are clearly visible, especially during the second half of the frame. The spacecraft was travelling at a velocity X(0.81, 25.09, -5.29) with orientation Λ(130.90, 292.25).

5.4. Frame 11391.53 (Figure 6; Figure 11)

This frame was acquired when the spacecraft was at R(4.13, 0.40, 293.38), near the outbound ringplane crossing. A large number of impacts are visible in the Figures, especially in the second half of the frame. The spacecraft's velocity was X(8.87, 16.91, -7.10), and its orientation was Λ(106.10, 218.65).

6. EVIDENCE FOR DUST IMPACTS

Why do we identify the events shown on the high rate frames under consideration as being the result of dust impacts? There are two basic reasons:

1. Although the PRA instrument had never before been operated in its high rate mode through periods in which dust was impacting the spacecraft, it has long been known that the PRA responds to dust impacts in its low rate mode. Therefore it is reasonable to expect that the high rate mode will also respond to dust impacts, unless the signal strengths caused by dust impacts are too low to rise above the increased background noise level of the high rate mode;

2. The relative number of events observable on the five frames under consideration mirrors exactly what would is expected if the impulses are caused by dust impacts (i.e.: few far from the planet; most intense at inbound ring plane crossing; a small number near closest approach; a relatively large number near outbound ring plane crossing).

In addition, each impulse in the data is a reasonable duration to represent an impact, and the wide variability in intensity and the stochastic nature of the event distribution indicates that it is a natural phenomenon, not merely some kind of unique onboard interference.

7. CALIBRATED AND UNCALIBRATED DATA

The data returned to ground are in the form of eight bit quantities (i.e. any single datum takes on a value between zero and 255 inclusive). Data values of zero and 255 are generally regarded as "bad data" and ignored. Data values in the range from unity to 254 inclusive are "looked-up" in a table and converted to millibels above a known zero level (which corresplonds to one microvolt across the front end of the receiver). The conversions between eight bit data numbers and sixteen bit millibel values are non-linear. Generally speaking, low values for the raw data numbers ("DN") correspond to millibel values of between 1400 and 2000. The very highest DN values correspond to calibrated values going as high as 8000 millibels.

7.1. DATA ANOMALIES

7.1.1. INVERTED DATA VALUES

There is a significant anomaly apparent in some of the uncalibrated data. A close look at Figures 2 through 6 shows that data acquired in the first half of the frame in the highest frequency channel (i.e. 900 kHz) have the bizarre property that when an impact occurs, the data numbers *drop* in value. This phenomenon occurs consistently throughout all five frames. Clearly, such an occurrence (signals dropping below the ambient noise level) does not represent a valid measurement of physical processes occurring during the time that an impact is affecting the PRA instrument. Surprisingly, Pedersen *et al.* (1991) make no mention of this problem during their somewhat cursory examination of high rate PRA data.

There are, *a priori*, several possible sources for this anomaly:

1. An unknown interaction within the PRA receiver;

2. A problem in the onboard computers;

3. A problem with the data processing that occurs before the data are delivered to Boulder.

From our point of view (as end users of the data with limited access to Project personnel), items two and three above can be combined. We therefore consider two possible sources of the anomalous data: internal to the PRA experiment and external to it.

7.1.1.1. POSSIBILITY OF INTERNAL PRA ANOMALOUS BEHAVIOUR

The PRA receiver is, of course, not perfect. Like any radio receiver, it can respond in anomalous ways (by which we mean ways that were not part of its design specification) to signals appreciatively different from those to which it was designed to be exposed. Generally, radio receivers such as the PRA are well behaved except in the presence of strong signals, even if such signals are outside of the nominal frequency to which the receiver is currently tuned. (Although it is more difficult for such a response to occur if the strongly interfering signal is outside the frequency range which the receiver is designed to receive; in the PRA, this frequency range is from 1.2 kHz to about 45 MHz.)

"Anomalous" behavior (in the sense that the PRA registered the presence of signals at frequencies at which no signals were, in fact, present) was observed on several occasions near Jupiter encounter, when intense low frequency emissions mixed with internally generated signals to produce "shadows" of these low frequency emissions at high frequencies near 40 MHz. This effect was not unanticipated and in fact occured exactly under the circumstances in which it was most to be expected.

It is clear that this is not the phenomenon we are witnessing in this case. However, there is also precedent (concurrent precedent, in fact), for the apparent lowering of noise background when the PRA receiver is exposed to strong signals. Figure 13 shows a series of single channel measurements acquired by the PRA in its low rate POLLO mode around the time of Neptune inbound ringplane crossing. In this mode, the PRA

dwells for 30 milliseconds on a given channel, acquiring data by boxcar integration for the final 25 of those 30 milliseconds, and returns an 8 bit data number that encodes the integrated flux received during the 25 milklisecond integration period. The instrument then steps to the next lower frequency channel, except when it is already at the lowest frequency channel (1.2 kHz), in which case it jumps to the highest frequency channel and begins another sweep downward in frequency.

The data Figure 13 are from the very highest channels of the PRA receiver, around 40 MHz. In channel number three in particular (channels numbered 1 and 2 contain the status of the PRA instrument, not data), there is a clear *drop* in background signal strength at the time of ringplane crossing.

However, there are important differences between this unique phenomenon at very high frequencies in the instrument's low rate scanning mode and the high rate frames which are the subject of the instant study.

During the acquisition of a single data point on Figure 13, many, many dust impacts occur. Also, the amount of decrease to the apparent background signal level varies smoothly with the total number of impacts on the spacecraft (the gradual decrease in apparent background level is concommitant with approach to the maximum rate of impact). But in the high rate frames, we are examining single, individual impacts. And the noise level appears to drop even when the impact is barely under way, or during its extended tail. Thus, even at times when it is reasonable to believe that the instrument is being exposed to quite a small signal level, still the data show a clear decrease in perceived signal intensity.

If the data at 900 kHz are called into question in this way, then we must also wonder about those data acquired at other frequencies, which, even though they do not exhibit the same bizarre behaviour, must surely be contaminated to some extent. Fortunately, there is a test that we can apply to the 900 kHz data.

The PRA data can be calibrated and examined closely for signs of inconsistency. In particular, the instrument has a known response to rapidly varying signals of reasonable intensity (i.e. of insufficient intensity to produce nonlinear intermodulation distortion effects). The signal passes

through a simple RC circuit of time constant 100 microseconds before being sampled and digitised. Any data provided by the instrument should be in accord with the introduction of this time constant.

Because the instrument contains a simple RC circuit with a time constant of 100 microseconds at the front end, it is easy to calculate the instrumental response to an arbitrary pulse of energy within its passband.

Suppose that the background flux level is F_B and on this background is superposed a rectangular pulse of flux F_S which commences at time T_0 and ceases at time T_1. Then prior to the commencement of the pulse, the instrument returns some value of DN, N_1 which is constant and represents (if we ignore quantization errors and errors in measurement) the flux F_B.

Once the pulse begins (time δT between T_0 and T_1), then the output measurement N_2 is simply given by

$$N_2 = F_B + F_S\left(1-\exp\left(\frac{-\delta T}{100}\right)\right) \qquad (1)$$

Once the impulse has finished, then the output N_3 is given by

$$N_3 = F_B + F_S\left(1-\exp\left(\frac{(T_1-T_0)}{100}\right)\right)\exp\left(\frac{-(T-T_1)}{100}\right) \qquad (2)$$

where T is the time since the end of the impulse.

The PRA instrument is calibrated in terms of millibels, not linear power, and plots of PRA data are usually produced such that the ordinate is linear in millibels, not Watts. Therefore, we can say that the number of decibels above the background level corresponding to F_B at time T after the pulse has passed is given simply by

$$M = 10\log_{10}\left(1+F_S''\exp\left(\frac{-(T-T_1)}{100}\right)\right) \qquad (3)$$

where

F_S'' is $\left(\frac{F_S}{F_B}\left(1-\exp\left(\frac{(T_1-T_0)}{100}\right)\right)\exp\left(\frac{-(T-T_1)}{100}\right)\right)$,

which is simply the highest output of the instrument, seen at the time of the trailing edge of the pulse.

Now it is a trivial matter to calculate the instrument response to pulses of various intesities. Consider three cases, where the peak output of the instrument corrsponds to 5, 10 and 20 dB above background respectively. Figure 14 demonstrates the continuous instrument response to these three cases. When the impulse is intense, then the early part of the response is nearly linear, corresponding to a decay slope of -4.34 decibels per 100 microseconds, or -6.08 decibels for 140 microseconds, which is the duration between consecutive samples at a single frequency.

The PRA instrument does not sample and return continuously; it samples the signal every 140 microseconds, holds that value for digitisation and returns it to Earth (encoded as a data number). Consequently, once an intense impulse is completed, the fastest observable decay rate in the instrument corresponds to a roll off of -6.08 dB per sample, even if there is no emission whatsoever to measure during this time.

Thus, if a sudden, short signal is applied to the instrument, the data should show a quite rapid rise, followed by a less rapid decay as the capacitor discharges (relatively) slowly through the resistor. This is exactly what is seen when many of the cleanest signals at 600 kHz and 300 kHz are examined.

By way of example, consider Figure 15, which shows data from 600 kHz in a frame obtained during outbound ring plane crossing. The maximum negative gradient during this (very typical) dust impact is exactly what one would expect from a signal which was abruptly removed from the receiver. That is, it corresponds to the 100 microsecond time constant of the RC filter. Superimposed on the plot of the data stream are lines corresponding to the instrumental response to a suddenly removed intense signal. The decay gradient for the first peak in the data stream precisely matches this calculated gradient; the observed gradient of the second decay is slightly less steep than the calculated value. This behaviour is typical. Many impacts at 600 kHz have been examined, and no case has been found in which the decay of signal exceeds what is possible given the known time constant of the circuit; there are many impacts in which (like Figure 15) the decay occurs exactly at the expected maximum rate. Consequently, we assert that the calibration of data at 600 kHz (and also at 300 kHz) is valid,

although that at 900 kHz, for unknown reasons (but see below), is invalid.

7.1.1.2. POSSIBILITY OF ERROR IN DATA TAPES

The most likely form of data processing anomaly (or onboard computer glitch) is a simple subtraction of a data number from 255, although how this might occur is unknown. To test whether this has actually occured, we can simply subtract the data values at 900 kHz from 255, then apply a test similar to that above: do the decay gradients ever exceed that permitted by the 100 microsecond time constant of the circuit? The answer appears to be "no". In fact, just as for 600 (and 300) kHz, the maximum negative gradient is observed quite often, and appears to be identical to what one expects from the known characteristics of the circuit.

Consider Figure 16. Figure 16a shows a rather complicated dust impact as seen during inbound ringplane crossing at 600 kHz. (In fact, the most likely explanation for the data's complexity is that what is observed is a series of two impacts, one commencing near abscissa 21, and one commencing around abscissa 22.5). Figure 16b shows the corresponding *simultaneous* data in the 900 kHz channel, after the raw data have been subtracted from 255. The detailed structure of the data is quite different in the two channels. However, the maximum decay rate in the 900 kHz channel seems to be almost exactly what one expects from the PRA receiver if the data have been treated in this way. An examination of many other impacts has produced no example of a decay faster than predicted. Therefore, we conclude that somehow, by an unknown mechanism, the data for 900 kHz have been subtracted from 255 before being written to tape and sent to Boulder.

(One might question why other gradients are not considered: the rise gradient in the inverted data, and the rise and decay gradients in the raw data. The answers should be obvious on a moment's reflection. The raw data are, *a priori*, known to be bad; therefore no deduction other than, at most, a confirmation of the badness of the data is possible. The rising gradient also is not informative, since it is limited only by the strength of the signal from the impact, which is unknown.)

8. DETECTING IMPACTS IN THE DATA STREAM

When only a small number of events of a particular type are present in a given data stream, it is reasonable to produce a catalogue of such events manually. For large numbers of events, an automated program is required that recognises and catalogues each event. However, the construction of such a program to detect putative dust impacts as they appear in high rate PRA data is extremely difficult (if not impossible). There are two major reasons for this difficulty:

1. The signature of a single dust impact often contains substantial periods of time when the signal returns to the background level, only to rise again later in the impact signature;

2. While it is relatively simple to locate dust impacts when they are infrequent, at ring plane crossings there are many, many impacts per second; consequently it is almost impossible to determine a valid background level of spacecraft noise against which the impacts are to be detected.

Consequently, it has been found to be most efficient to count impact signatures by manually. When the impact rates are at their highest, it is simply impossible to count impacts by any means. The duration of a typical impact at such times is longer than the time between impacts, and so it becomes simply impossible to distinguish individual impacts in the data. Figure 17 was acquired shortly before inbound ring plane crossing; it is clearly impossible to make any other than the crudest estimate of the number of impacts in these data.

9. COMPARISON OF PWS AND PRA EXPERIMENTS

The PWS and PRA experiments are the only two experiments aboard Voyager that have detected the results of dust impacting the spacecraft. Neither instrument was designed as a dust counter and, although there are similarities between the two experiments, there are are also differences that it is important to understand when trying to compare the measurements from the two instruments.

Both are nominally radio experiments, measuring a signal

obtained on a pair of antennas which is then processed by the instrument and the FDS; resulting data numbers are then returned to Earth. The two experiments share a pair of antennas, two copper-beryllium tubes, each 10 metres long and half an inch in diameter, arranged orthogonal to one another and attached to the spacecraft bus. However, the feed arrangement is different for the two experiments. The PWS experiment uses the antennas as if they were a dipole; that is, it responds to the instantaneous voltage difference presented by the two antennas at the point where they converge on the instrument. The PRA uses the antennas as a pair of orthogonal monopoles mounted against the spacecraft. Further, when detecting dust impacts, the PWS samples the actual voltage on the antennas from moment to moment (four bit samples are acquired every 35 microseconds). An automatic gain control is built into the instrument. This has a time constant of approximately 0.5 seconds (Gurnett *et al.*, 1991) and so has little effect on the detection of impacts, which occur on much shorter time scales. However, the impact signatures vary over a large range in intensity, and many of the more intense impacts saturate the instrument; during the recovery phase (which may last for many milliseconds) the instrument is incapable of properly detecting further impacts, so that a substantial fraction of dust impacts go undetected. The correction ration (total estimated impact rate to detected impact rate) is roughly 1.58 at the inbound and roughly 1.37 at the outbound ring plane crossings respectively.

Figure 18 shows typical signatures for a number of impacts, as they appear in PWS data.

The PRA instrument does not respond directly to the voltage on the antennas. Instead, it responds to rapid fluctuations in that voltage; that is, it returns the flux density across a given bandwidth. Thus, it is theoretically possible for PWS to return a large signal when PRA returns no signal (i.e. when a large, but relatively slowly varying voltage appears across the two antennas); the converse is also possible (a relatively small overall voltage is induced, but it fluctuates very rapidly). Thus, the two instruments, if their measurements are understood properly, are in some ways complementary.

Prior to Neptune encounter, no high rate measurments of dust impacts had been made by the PRA instrument, although many such measurements were available for the PWS instrument. At this time, it was unknown what signature individual dust impacts had

in the PRA instrument, and workers had to rely on the integrated measurements obtained in low rate modes. The rise time of the impacts in Figure 18 is very short, limited by the bandpass filter used in the PWS wideband receiver; in particular, it is shorter than than the 35 microsecond sampling period; the fact that PRA was detecting dust impacts (even in low rate data) as high in frequency as 1 MHz was taken as evidence that the initial rise time of the pulse was as short as 1 microsecond.

However, if the source of the PRA signal were indeed the Fourier component of the rise time of the voltage pulse detected by PWS (which, *a priori*, was a reasonable assumption) then the high rate signatures would look quite different from those actually found at Neptune. If the hypothesis were correct, PRA would have detected a single pulse corresponding to the start of a voltage pulse, followed by a CR dominated decay like those in Figure 14. Although some events have this general appearance, the vast majority do not, displaying instead a duration considerably longer than would be expected by this hypothesis (in fact, the duration of events detected by PRA seems to be no shorter than that of events detected by PWS, see below), as well as displaying considerable internal structure within each pulse. Consequently, we conclude that the PRA measurements do not correspond to a simple Fourier compnent of a rapidly rising voltage, but instead reflect ongoing plasma oscillations within the expanding plasma cloud (see below).

10. THE APPEARANCE OF "TYPICAL" EVENTS

Figure 20 shows a number of typical impulsive events recorded in the high rate frames throughout the encounter period. Many (but by no means all) events have a characteristic structure:

1. Sudden onset, rising as quickly as the 100 microsecond RC circuit will permit, to a maximal value;

2. A rapid decline after a small number of samples (often only one) from this value at a rate limited by the 100 microsecond time constant;

3. A period of relative quiescence, in which the returned data numbers are at (or near) background

levels;

4. A rapid rise to a second peak; usually this rise is not limited by the time constant of the circuit; neither is it as high as the first peak;

5. A broad peak which drops smoothly to background levels relatively slowly;

6. The entire event typically lasts from 8 to 16 samples (1.12 to 2.24 milliseconds).

Other impacts display variations on this theme; sometimes one peak is missing; sometimes the structure is more complex, with a greater number of peaks than the two described above. However, the description above covers the greatest number of events, and so we shall use it as a canonical norm as we attempt to understand the physics underlying the observations.

11. PRA AND PWS IMPACT RATES

High rate PWS and high rate PRA data acquisition are mutually exclusive modes of operation for Voyager. Therefore, it is not possible simply to compare, on a moment by moment basis, the two data sets. However, the PWS experiment operated in its high rate mode for a vastly greater portion of the encounter than did the PRA instrument. It is therefore relatively easy to interpolate between PWS data frames to determine impact rates that PWS would have found had it in fact been operating simultaneously with the PRA high rate measurements.

Figure 19 shows the periods of acquisition of PRA and PWS frames.

As explained above (see also Figure 17), it is not always possible to determine the impact rate from the PRA observations. PWS is not so limited. The reasons for this are several (and, some may argue, somewhat suspect). PWS counts impacts by using an automatic detection scheme, rendered necessary by the large number of high rate frames of PWS data acquired throughout the encounter period. An event is signalled by a characteristic signature within the PWS data. A "dead time" is then imposed following the event, during which data are ignored. This dead time is then allowed for in

calculating the effective number of impacts. Without physical access to the PWS data, it is impossible to determine how frequently those data show impacts crowded atop one another; neither do the team describe how their detection and counting algorithms respond to such a situation. The peak impact rate according to PWS is roughly 450 actual (as opposed to detected) impacts per second.

In every instance where we compare the actual number of PRA detections with the interpolated number of PWS detections, we find that the former represents only a fraction of the latter. For example, consider the inbound ring plane crossing. Figure 21 shows the impact rate inferred by PWS during the period of inbound ring plane crossing. The solid line is a best fit to the equation

$$R = R_0 + R_1 \exp\left(\frac{-(z-h)^2}{\Delta z_1^2}\right) + R_2 \exp\left(\frac{-(z-h)^2}{\Delta z_2^2}\right) \qquad (4)$$

where
h is the offset from the symmetry axis from the equatorial plane;
Δz is the half thickness of the respective gaussian component.

Gurnett *et al.* determine the numerical values of the various constants in this equation to be: $R_0 = 77\ s^{-1}$, $R_1 = 241\ s^{-1}$, $R_2 = 103\ s^{-1}$, $h = 146$ km, $\Delta z_1 = 268$ km, $\Delta z_2 = 921$ km.

(The dotted line in Figure 21 represents the same curve shifted by 180 km, for use with the PRA ephemeris.)

A similar situation exists at outbound ring plane crossing (Figure 22), except that in this case the form of the best fit line to the PWS data is considerably simpler:

$$R = R_0 + R_1 \exp\left(\frac{-(z-h)^2}{\Delta z_1^2}\right) \qquad (5)$$

with: $R_0 = 91\ s^{-1}$, $R_1 = 53\ s^{-1}$, $h = 948$ km, $\Delta z_1 = 1036$ km,

(As an aside, the value of dead time in the PWS instrument is, surprisingly, considerably higher during the outbound ring

plane crossing than during the inbound one).

One difficulty in comparing counting rates is that the ephemeris used by the PWS team clearly differs from the one used by PRA. This is not a surprise; before, during and after an encounter, a variety of spaecraft ephemeris tapes are issued, and discrepancies from one tape to the next are quite common as he determination of the spacecraft's actual position changes over time. The PWS team uses a tape in which the predicted ring plane crossing (distance from equator == 0) occurs almost exactly at 0253. The ephemeris used by the PRA team places passage through z = 0 at 0252 and 40 seconds, about 20 seconds prior to that of the PWS ephemeris. Consequently, predicted impact counts have to be shifted by 20 seconds, or approximately 180 km in the vertical direction. Thus, we can use formula 4 above, but we must substitute the value h = 146 + 180 == 326 km in the formula.

We can use formulas 4 and 5 to calculate predicted impact rates that PWS would have detected had it in fact been able to return data simultaneously with the PRA instrument. Figure 23 shows impact rates as determined from PRA data for the frame 11388.56, at 600 kHz. The increase in impact rate as ring plane is approached is obvious. This close to the ring plane, however, the PWS predicts much higher impact rates. The dotted line on the figure is one-third the predicted PWS impact rate. This gives roughly the right number of impacts as detected by PRA, but the PRA data indicate a much more rapidly rising impact rate than the PWS data. One plausible explanation for this is that only certain particles create signatures detectable by PRA, and the fraction of the total population that comprises such particles increases near the ring plane.

Figures 24 through 27 show various impact geometries. Although it is unlikely, it is possible, *a priori* for at least some fraction of the dust particles orbiting the planet to be moving in a retrograde motion. (That the bulk of the particles moves prograde can be immediately deduced from the apparent motion of the neptunian ring arcs.) Indeed, the presence of Triton, a large, retrograde satellite, renders the gravitational heating of the particle cloud likely. (This is probably the reason why the entire neptunian environment is dusty, instead of the particles being confined to a thin ring, as at other planets.) Consequently the Figures depict the spacecraft as it would be viewed at the ring plane crossings by both prograde and retrograde particles in circular keplerian orbits.

In all these geometries, the fraction of the total visible projected spacecraft occupied by the antennas is quite small, being 6.7%, 9.0%, 7.4% and 8.7% respectively for the four cases inbound prograde, inbound retrograde, outbound prograde and outbound retrograde. Since it seems highly unlikely that PWS would be capable simultaneously of detecting events on the spacecraft body while missing impacts on the antennas themselves which are detected by PRA, we conclude that PRA, like PWS, detects events from all over the spacecraft. We note that if the difference in detected rates were to be due simply to compositional differences across the spacecraft, then the ratio of detected impact rate for PRA and PWS should be roughly constant, as the impact geomety does not change perceptibly during the duration of Figure 23. The fact that the ratio is not constant indicates that the mechanism is more likely to be due to a change in the population of particles capable of being detected by PRA as the spacecraft approached the ring plane.

12. THE PHYSICS OF DUST IMPACTS

Surprisingly, the physics undergirding the observations of dust impacts on Voyager, even after three planetary encounters which exhibit such impacts, is not well thought out. By extrapolation from terrestrial laboratory experiments, estimates of particle size and mass distributions have been made, but no attempt has been made to predict or understand the appearance of dust impacts in the PRA high rate data. The single prediction referred to above is clearly in error.

The best authority in the literature regarding the physics of high speed dust impacts appears to be by Drapatz and Michel (1974), from which much of the following is derived.

12.1. CHANGES OF STATE

When a high speed particle impacts a solid object, some rather complicated physics occurs. Exactly what happens depends on a number of factors, including: the velocity of the impact, the purity of the particle and the impacted object, the chemical composition of both particle and impacted object, and the environment surrounding the impact site. The last of these is particularly simple for the cases which here concern us: the environment is simply a vacuum.

As a particle begins to impact an object, an initial sequence of shock waves commence to propagate through both materials, thus heating them. In the impacted object, these shock waves can propagate outwards relatively freely, away from the impact site. In the dust particle, the trailing edge of the particle imposes a strict boundary, at which the waves are reflected, effectively heating the material of the particle even more. For the high speed impacts with which we are concerned, sufficient energy is concentrated in these waves for heating, then evaporation, to occur quickly, primarily in the particle, but also (to some extent) in the spacecraft body as well. Thus, for a short period of time, a small ball of very hot gas is created. The temperature of this gas typically ranges from 10^4 to 10^5 kelvins. Some fraction of this gas, following the Saha equation, becomes ionised. Although global charge neutrailty must be conserved, Drapatz and Michel state that the ions and the electrons are thermally decoupled. If T_e is the electron temperature and n_e is the electron density, they show in their equation (12)

$$\frac{dE_c}{dt} = -ikT_e \frac{d\ln n_e}{dt} \qquad (6)$$

There is therefore an electron gas (of both free and bound electrons) which is both cooled by expansion into the surrounding vacuum and heated by the recombination and deexcitation of the electrons. The mean free path of the electrons is greater than the size of the interior ion cloudlets. However, because the electrons are lighter than the ions, some will escape the immediate vicinity of the cloudlet, producing a structure roughly like a spherical (if one ignores the spacecraft body), expanding capacitor with positive on the onner sphere and negative charge on the outer. In this situation, those electrons which now attempt to escape the innermost region will meet a potential wall created by the ions they are leaving behind and the electrons ahead of them. Therefore, the electrons near the leading edge of the expanding ion cloud are subject to strong electrostatic forces which accelerate them and thus are capable of creating the kinds of signals detected by the PRA instrument. Note that these are *not* freely propagating waves, but *in situ* plasma excitations of a rather nonstandard sort.

As the cloud expands, the degree of ionization initially drops rapidly because of recombination, but the cloud quickly

(within a nanosecond or so) reaches a point where the collision frequency becomes negligible and the degree of ionisation of the cloud remains effectively constant thereafter. Drapatz and Michel solve the equations numerically and show that the typical remnant ionisation of the cloud as it continues to expand into the vacuum is of the order of ten percent. It is simple to calculate the approximate velocity of expansion of the cloud. This is basically the expansion of neutral carbon atoms at 10^5 kelvins. The expanding cloud does no work, and so its temperature remains constant as it expands. Thus, there is an expanding plasma cloud, in which the leading edge comprises electrons which are accelerated by neighbouring electrons and the (relatively) slowly expanding ion core. These forces cause the electron cloud to expand at roughly the same rate as the ion cloud (so that quasi-local charge quasi-neutrality is maintained in the plasma). Figure 28 shows the maxwellian velocity distribution that corresponds to this scenario. A typical ionic velocity can be simply calculated from the equation:

$$\frac{3}{2}kt = \frac{1}{2}mv^2$$

For the case in point, a typical ion travels at a little over 14 kilometres per second with respect to the spacecraft. Thus, it crosses a typical dimenesion of the PRA antennas (of 10 metres) in about three quarters of a millisecond, which is the typical period between peaks in the signatures of dust impacts. Thus, the PRA data are consistent with an expanding cloud of plasma created by ionisation when a dust particle impacts the spacecraft, is raised to a temperature of some 100,000 kelvins and then expands into the vacuum.

13. ACKNOWLEDGEMENTS

I acknowledge R. L. Poynter of the Jet Propulsion Laboratory for his confirmation that the PRA high rate configuration during Neptune encounter was indeed as depicted in Figure 1. Nick King of Radiophysics is acknowledged and gratefully thanked for his work in programming the spacecraft views contained herein in the Mathematica programming language (Figures 24, 25, 26 and 27).

FIGURES

1. A pictorial representation of the configuration of the PRA experiment for high rate frames throughout the Neptune encounter.

2. Frame 11386.08, acquired some eight and a half planetary radii above the cloudtops. Raw data are plotted. A single dust impact is visible near the end of the frame as a narrow vertical line in both channels. Within each strip, data values run from zero to 255.

3. Frame 11388.56, acquired near inbound ringplane crossing. Raw data are plotted. A large number of dust impacts are visible. Within each strip, data values run from zero to 255.

4. Frame 11388.57, acquired near inbound ringplane crossing. Raw data are plotted. A large number of dust impacts are visible. Within each strip, data values run from zero to 255.

5. Frame 11390.38, acquired near closest approach. Raw data are plotted. Even though the spacecraft is close to the planet and far from the ringplane, several dust impacts are visible. Within each strip, data values run from zero to 255.

6. Frame 11391.53, acquired near outbound ringplane crossing. Raw data are plotted. A large number of dust impacts are visible. Within each strip, data values run from zero to 255.

7. Frame 11386.08. Calibrated data are plotted. Within the upper two strips, data run from zero dB to 80 dB above a calibrated zero point; the lowest strip depicts polarisation.

8. Frame 11388.56. Calibrated data are plotted. Within the upper two strips, data run from zero dB to 80 dB above a calibrated zero point; the lowest strip depicts polarisation.

9. Frame 11388.57. Calibrated data are plotted. Within the upper two strips, data run from zero dB to 80 dB above a calibrated zero point; the lowest strip depicts polarisation.

10. Frame 11390.38. Calibrated data are plotted. Within the upper two strips, data run from zero dB to 80 dB above a calibrated zero point; the lowest strip depicts polarisation.

11. Frame 11391.53. Calibrated data are plotted. Within the

upper two strips, data run from zero dB to 80 dB above a calibrated zero point; the lowest strip depicts polarisation.

12. A high resolution plot of the single impact spike in frame 11386.08. The duration of the plot is 20 milliseconds. The data are raw, uncalibrated data numbers; the ordinate ranges from zero to 255. This was the first dust impact to be detected by PRA in its high rate mode. Measurements at 300 kHz and 600 kHz (each with 200 kHz bandwidth) are shown. The essential features of the impact occur simultaneously in both channels.

13. A plot of VHF data near 40 MHz acquired by the PRA in low rate POLLO scanning mode around Neptune inbound ringplane crossing. PRA channel numbers are at the extreme left edge of the Figure. Channel 3 is the highest frequency channel which contains valid data, and corresponds to a frequency of 41.262 MHz. Each successive channel is lower in frequency by 307.2 kHz. Each strip runs from 0 to 255 DN. The peak rate of dust impact determined by PWS occured at approximately two hours, 53 minutes and 15 seconds, at the same time (to known accuracy of time) as the maximum dip in background noise in the Figure. Ring plane crossing occured some 15 seconds prior to this.

14. Graph showing the response of the PRA instrument (operating in high rate mode) to signals which are removed abruptly. The response curves are for a simple RC circuit with a time constant of 100 microseconds.

15. A plot of 600 kHz data acquired during the outbound ring plane crossing. The points inside rectangles are data numbers from the instrument, the lines joining the crosses and diamonds represent the instrument response to a strong signal which is instantaneously removed from the antenna terminals. The first spike in the impact decays at exactly the maximum rate permitted by the instrumental response; the decay from the second spike is slower.

16. Decay rates for simultaneous data acquired near inbound ring plane crossing: a) at 600 kHz; b) at 900 kHz, with all data numbers subtracted from 255.

17. Raw data acquired near inbound ring plane crossing at 600 kHz. These data are some of the closest to the time of ring plane crossing. They demonstrate the impossibility of determining, either manually or by machine, the peak impact

rate in the PRA data.

18. Signatures of a number of impacts as they appear in PWS data.

19. The periods of acquisition of PWS andf PRA data: a) near inbound ringlane crossing; b) near outbound ringplane crossing.

20. Typical impacts in PRA high rate data.

21. Best fit curve of impact rates from PWS data (inbound ringplane crossing).

22. Best fit curve of impact rates from PWS data (outbound ringplane crossing).

23. Impact rates as the spacecraft approached inbound ringplane crossing. The ordinate is in impacts per second, the abscissa is distance in the vertical direction from ring plane. The curve is one third the values predicted by equation 4, obtained from PWS data.

24. The spacecraft as seen by a prograde orbiting particle during inbound ring plane crossing.

25. The spacecraft as seen by a retrograde orbiting particle during inbound ring plane crossing.

26. The spacecraft as seen by a prograde orbiting particle during outbound ring plane crossing.

27. The spacecraft as seen by a retrograde orbiting particle during outbound ring plane crossing.

28. Maxwellian velocity distribution for carbon particles at a temperature of 100,000 kelvins. Abscissa is speed in metres per second. Typical speeds are of the order of 15 kilometres per second.

REFERENCES

Drapatz S. and K. W. Michel, "Theory of Shock-Wave Ionization upon High-Velocity Impact of Micrometeorites", *Z. Naturforsch*, **29a**, p.870 (1974).

Gurnett D. A., W. S. Kurth, F. L. Scarf, R. L. Poynter, "First Plasma Wave Observations at Uranus", *Science*, **233**, p. 106 (1986).

Gurnett, D. A., W. S. Kurth, L. J. Granroth, S. C. Allendorf, R. L. Poynter, "Micron-sized Particles Detected Near Neptune by the Voyager 2 Plasma Wave Instrument", *J. Geophys. Res.*, **96**, p. 19177 (1991).

Gurnett, D. A., W. S. Kurth, L. J. Granroth, I. H. Cairns, W. M. Macek, R. L. Poynter, S. L. Moses, F. V. Coroniti, C. F. Kennel, D. D. Barbosa, "Plasma Wave Observations at Neptune", *Adv. Space Res.*, **12**, p. (11)47 (1992).

Pedersen, B. M., N. Meyer-Vernet, M. G. Aubier, P. Zarka, "Dust Distribution Around Neptune: Grain Impacts Near the Ring Plane Measured by the Voyager Planetary Radio Astronomy Experiment", *J. Geophys. Res.*, **96**, p. 19187 (1991).

Pedersen, B. M., A. Lecacheux, P. Zarka, M. G. Aubier, M. L. Kaiser, M. D. Desch, "Phenomenology of Neptune's Radio Emissions observed by the Voyager Planetary Radio Astronomy Experiment", *J. Geophys. Res.*, **97**, p. 19201 (1992).

Scarf, F. L., D. A. Gurnett, W. S. Kurth, R. L. Poynter, "Voyager 2 Plasma Wave Observations at Saturn", *Science*, **215**, p. 587 (1982).

Warwick, J. W., D. R. Evans, J. H. Romig, J. K. Alexander, M. D. Desch, M. L. Kaiser, M. Aubier, Y. Leblanc, A. Lecacheux, B. M. Pedersen, "Planetary Radio Astronomy Observations from Voyager 2 Near Saturn", *Science*, **215**, p. 582 (1982).

Warwick, J. W., D. R. Evans, J. H. Romig, C. B. Loon, M. D. Desch, M. L. Kaiser, J. K. Alexander, T. D. Carr, D. H. Staelin, S. Gulkis, R. L. Poynter, M. Aubier, A. Boischot, Y. Leblanc, A. Lecacheux, B. M. Pedersen, P. Zarka, "Voyager 2 Radio Observations of Uranus", *Science*, **233**, p. 102 (1986).

Warwick, J. W., D. R. Evans, G. R. Peltzer, R. G. Peltzer, J. H. Romig, C. B. Loon, A. C. Riddle, A. E. Schweitzer, M. D. Desch, M. L. Kaiser, W. M. Farrell, T. D. Carr, I. de Pater, D. H. Staelin, S. Gulkis, R. L. Poynter, A. Boischot, F. Genova, Y. Leblanc, A. Lecacheux, B. M. Pedersen, P. Zarka, "Voyager Planetary Radio Astronomy at Neptune", *Science*, **246**, p. 1498 (1989).

FDS Count	11386.08	11388.56	11388.57	11390.38	11391.53
SCET	89:237:0:36:47	89:237:2:51:11	89:237:2:51:59	89:237:4:4:47	89:237:5:12:4
Distance (Rn)	9.52	3.50	3.50	1.29	4.13
Latitude (°)	-17.88	-0.38	-0.38	61.15	0.40
Longitude (°)	6.35	60.61	60.61	244.60	293.38
Vx (km/s)	-18.16	-17.23	-17.23	1.22	17.11
Vy (km/s)	22.50	9.66	9.66	46.70	11.17
Vz (km/s)	8.42	8.92	8.92	-2.76	6.32
Θ (°)	51.32	69.28	69.28	130.90	106.10
Φ (°)	63.45	62.70	62.70	292.25	218.65

Table 1

PRA HR Neptune configuration

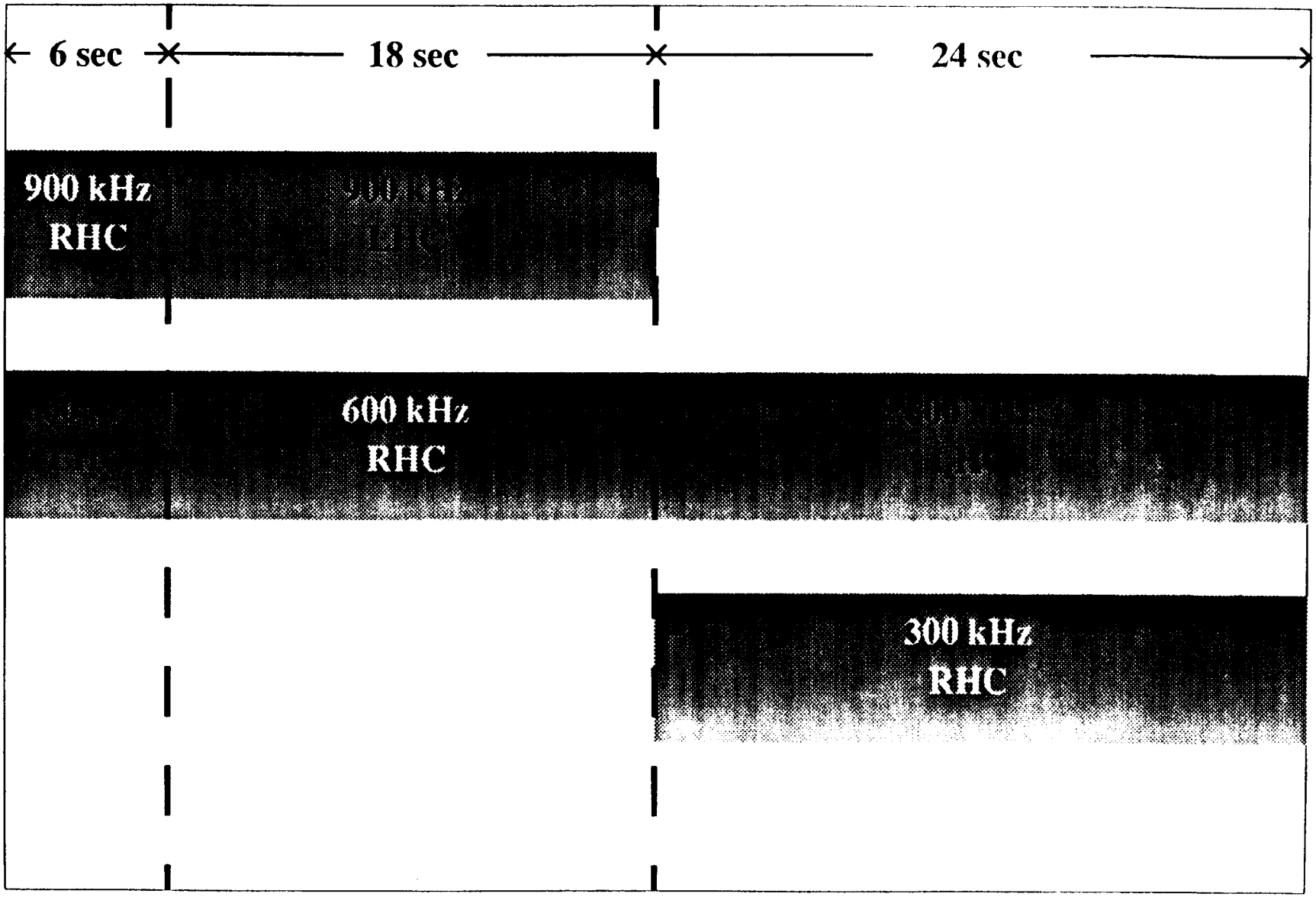

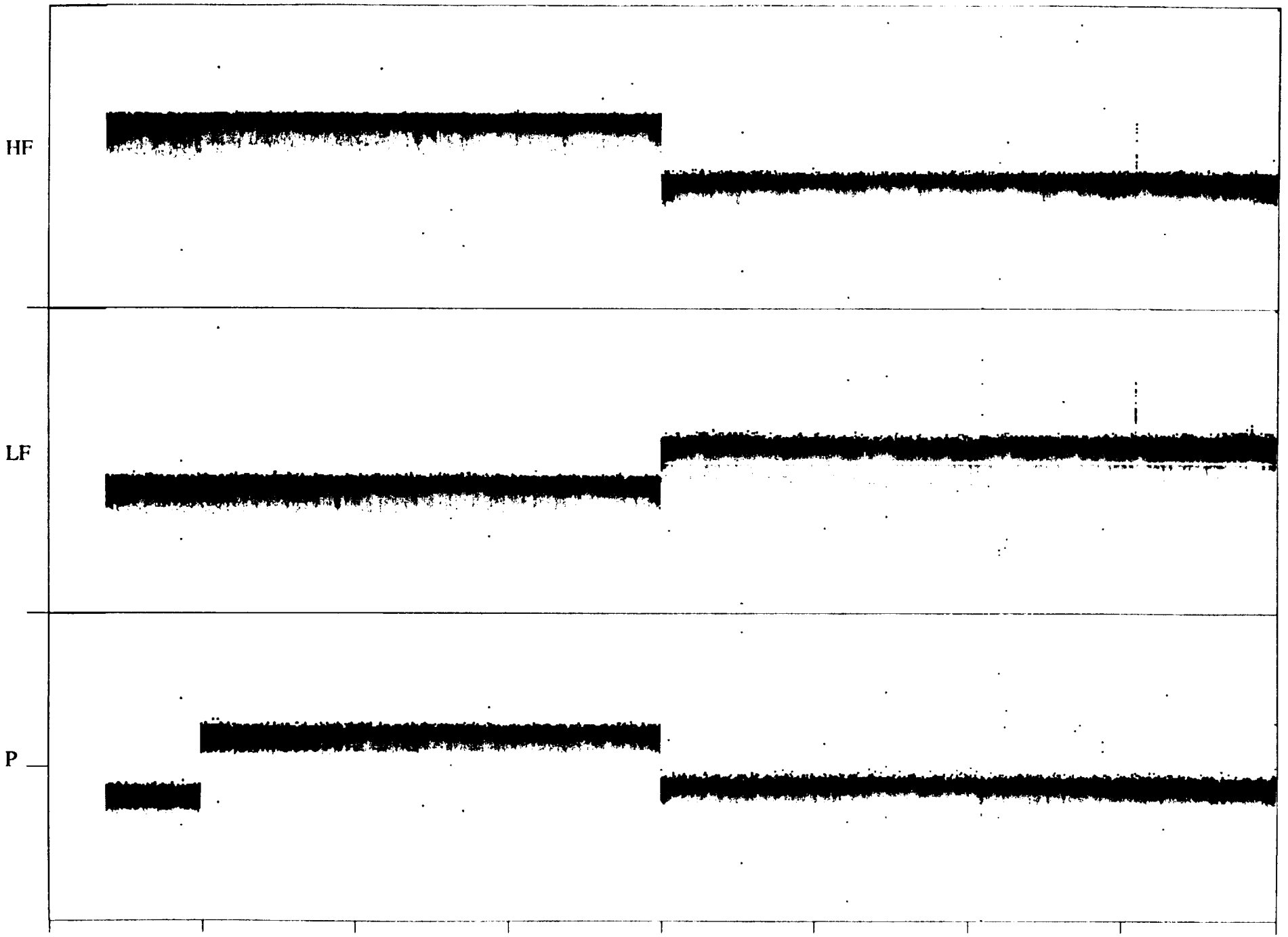

Figure 2

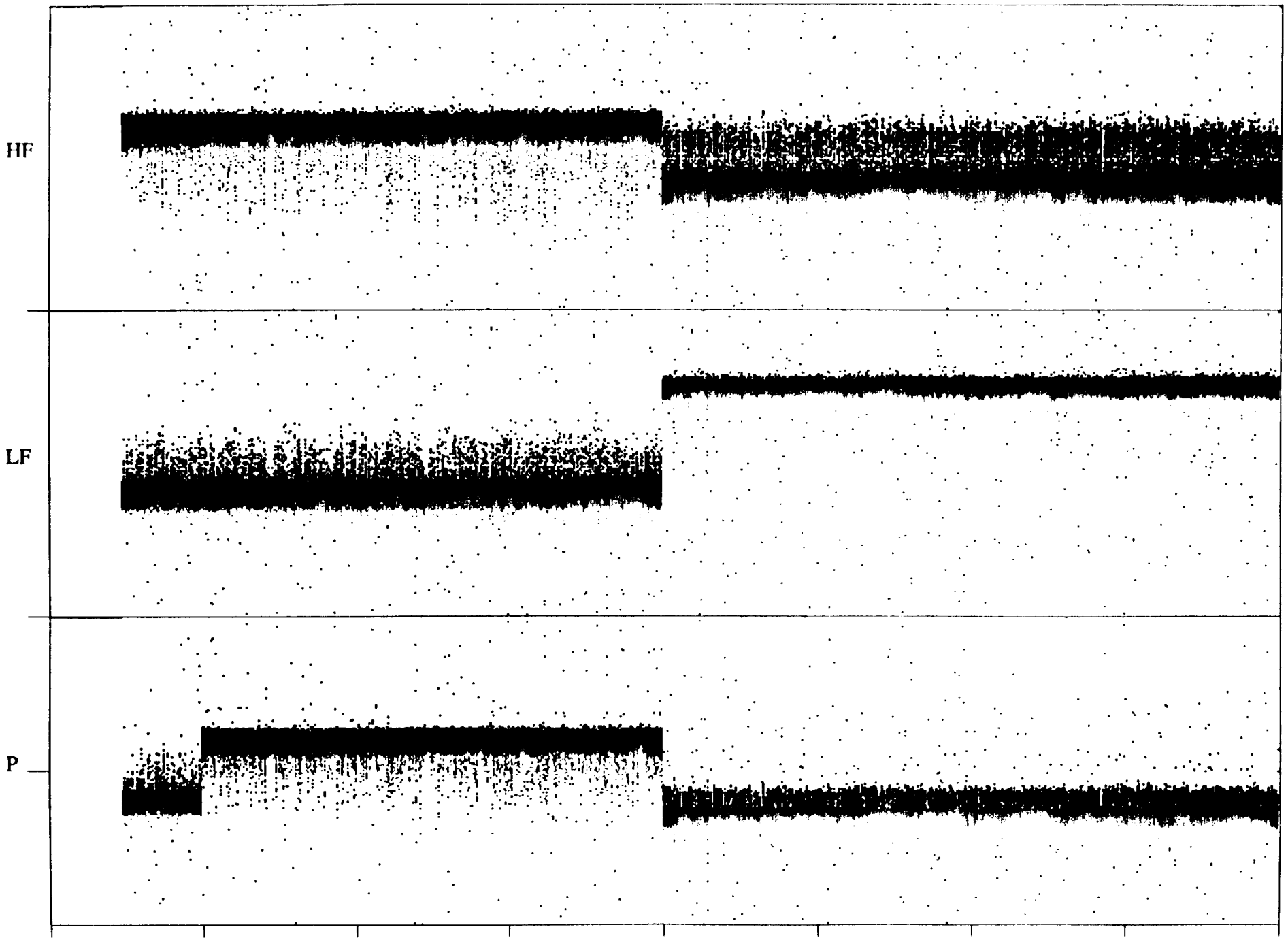

Figure 2

VOYAGER 2 11388.57 89:237:2:51:59

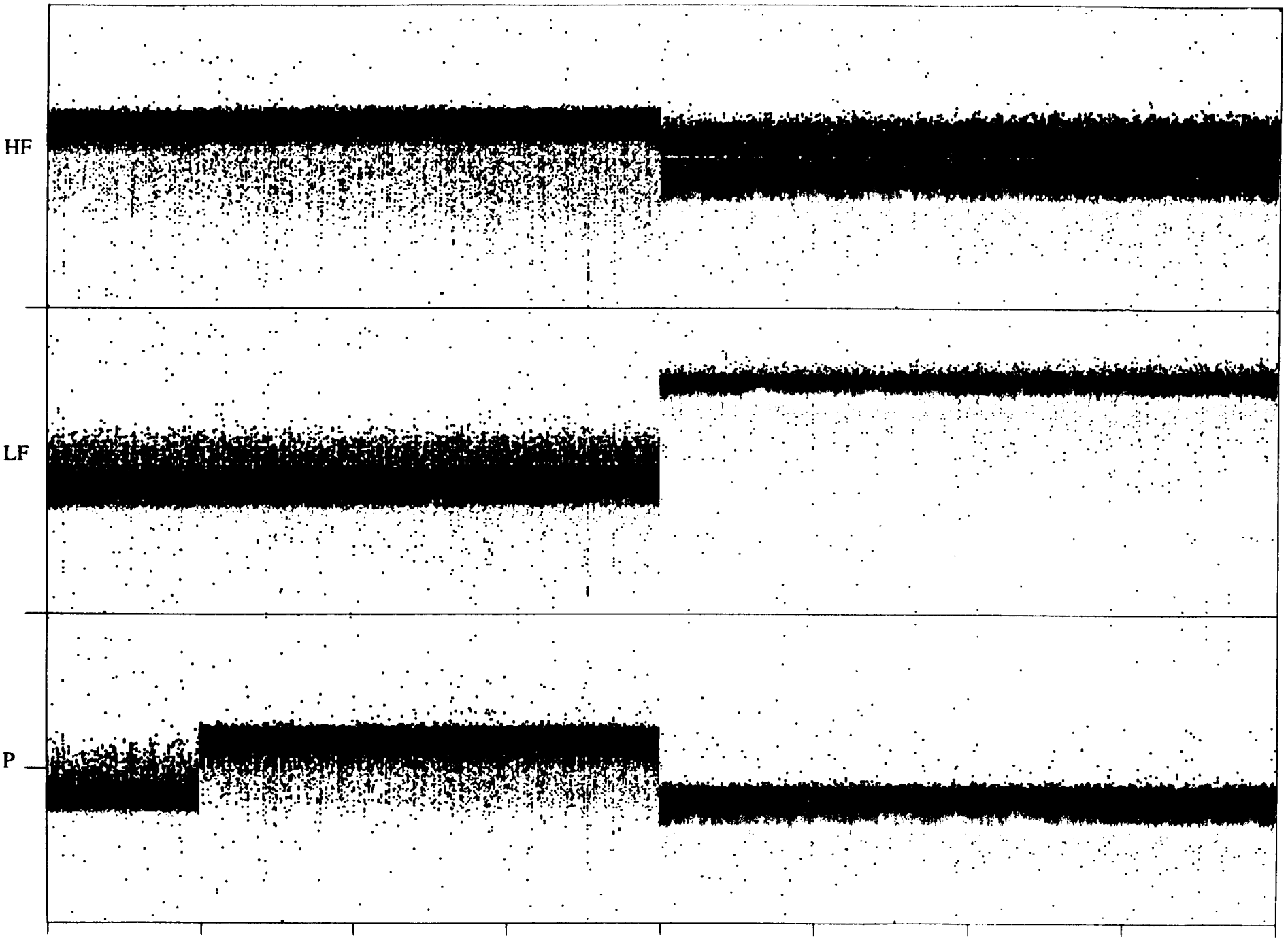

Figure 4

VOYAGER 2 11390.28 89:237:4:4:47

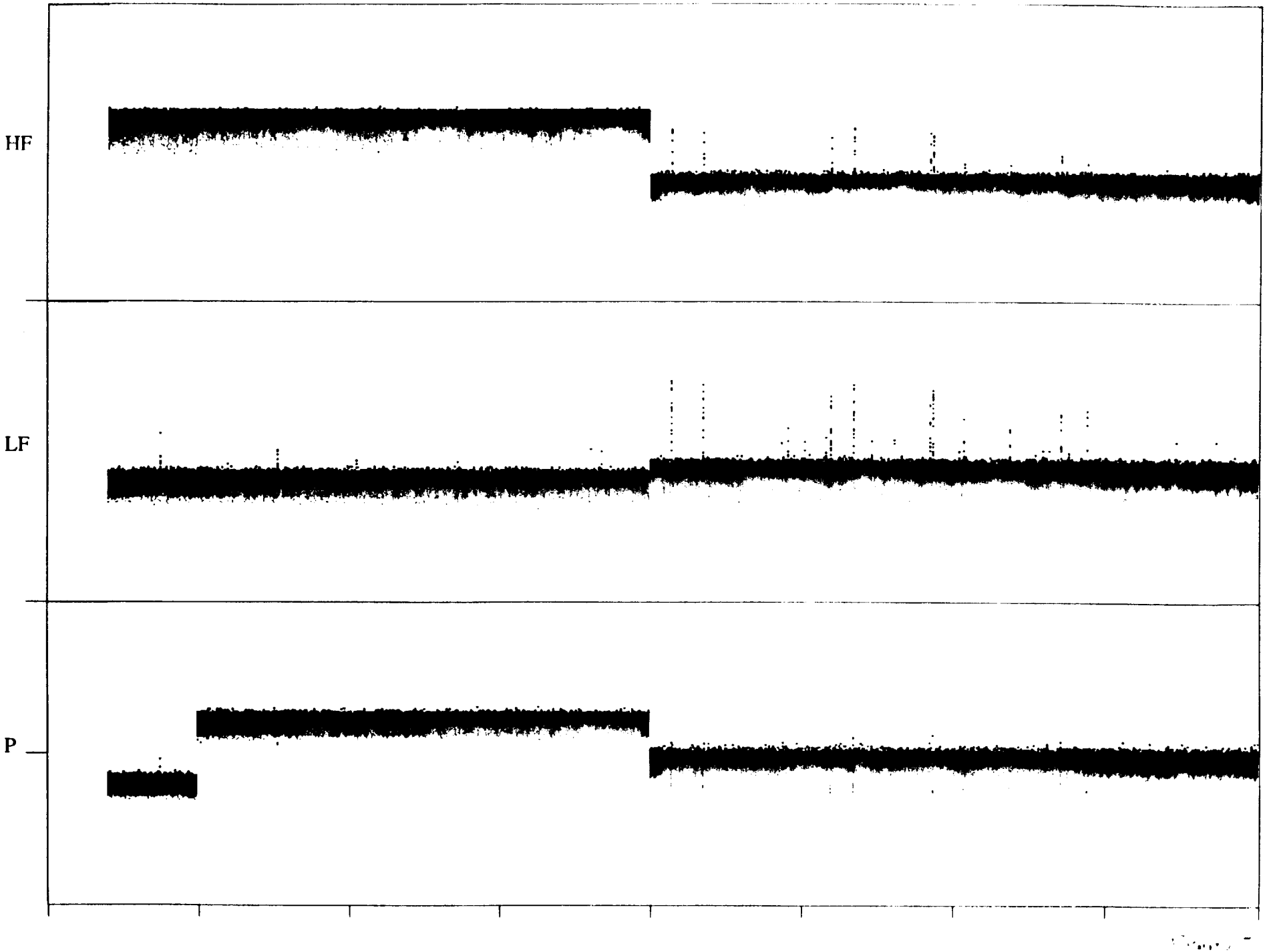

VOYAGER 2 11391.53 89:237:5:12:47

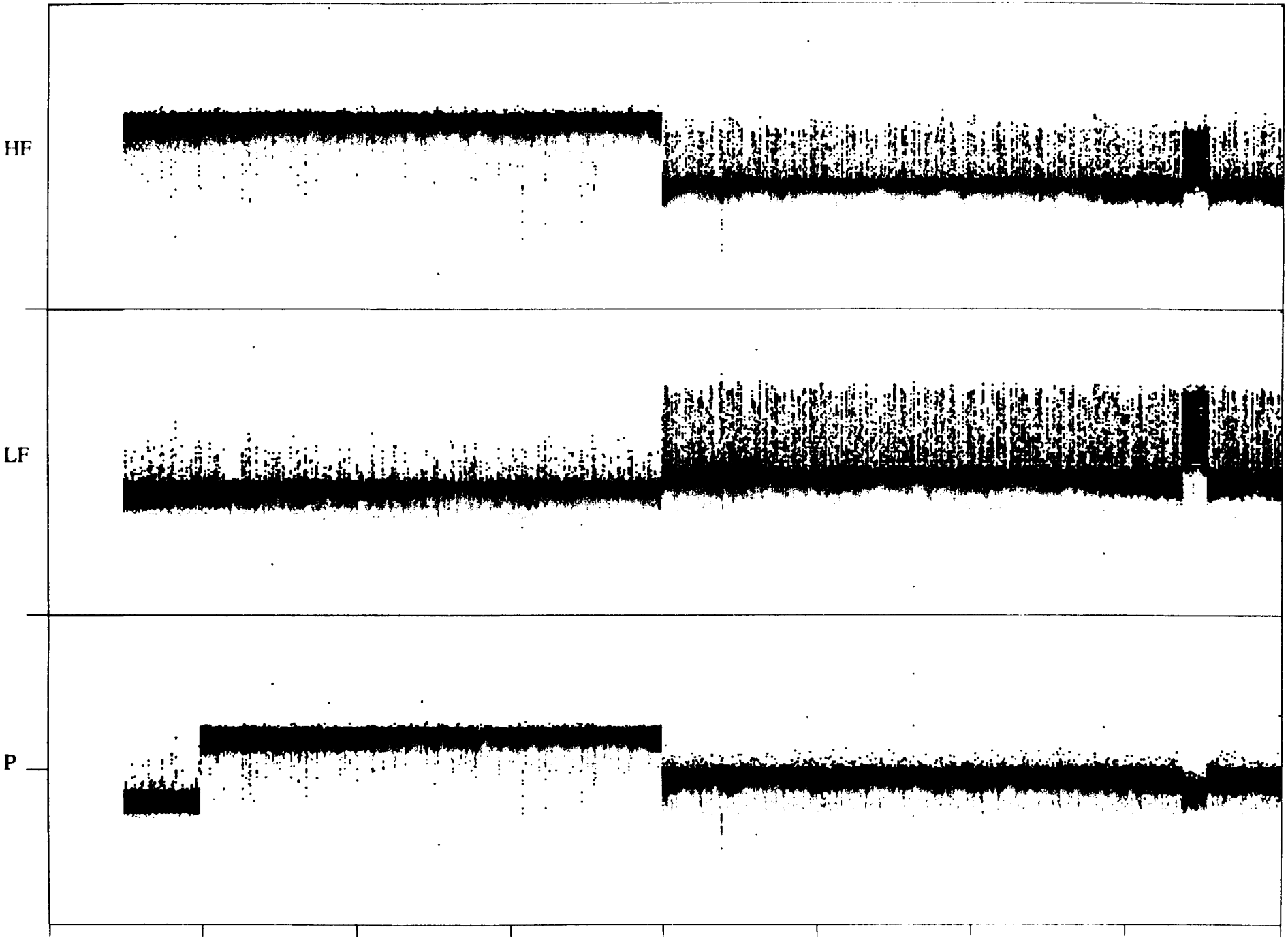

Figure 6

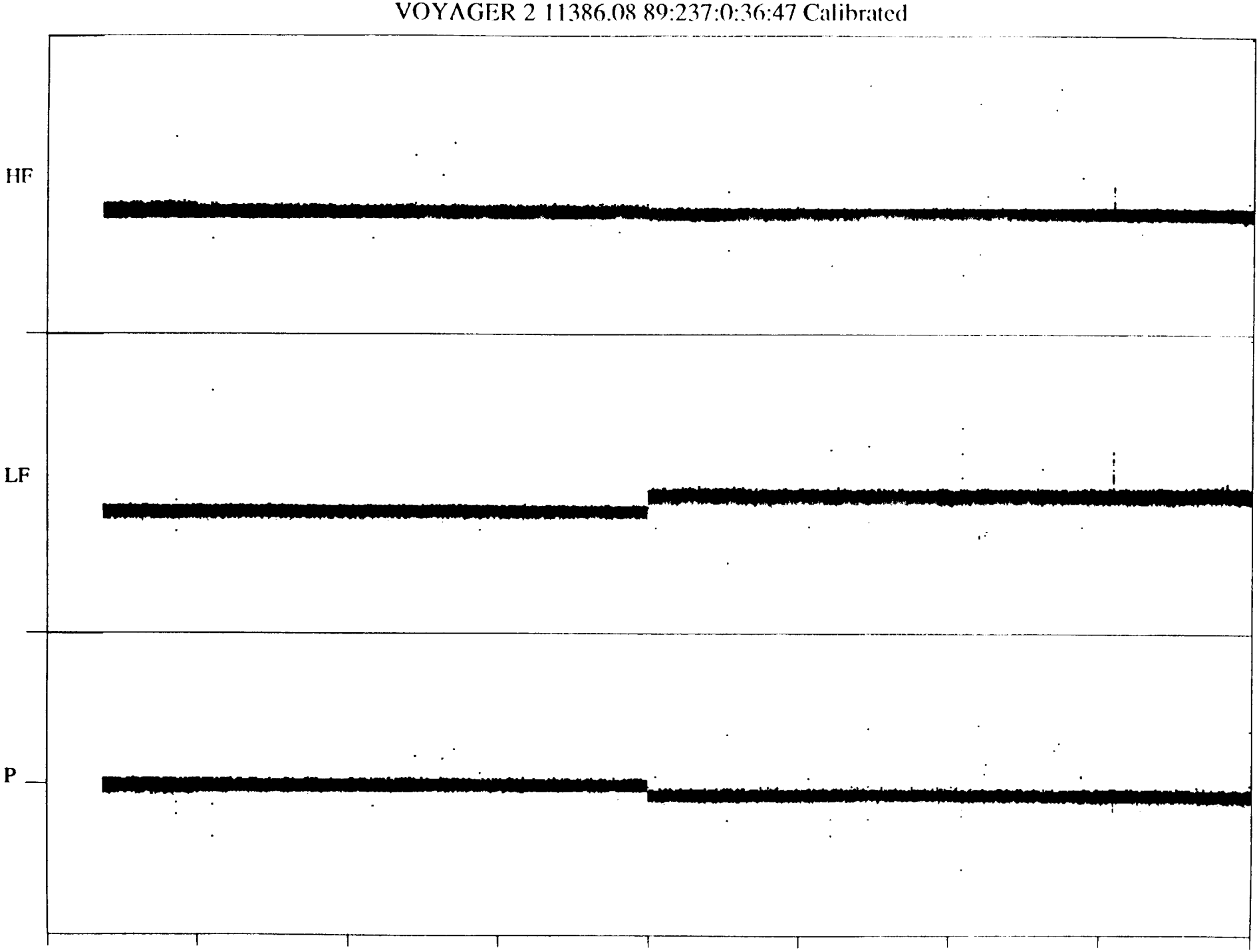

Figure 7

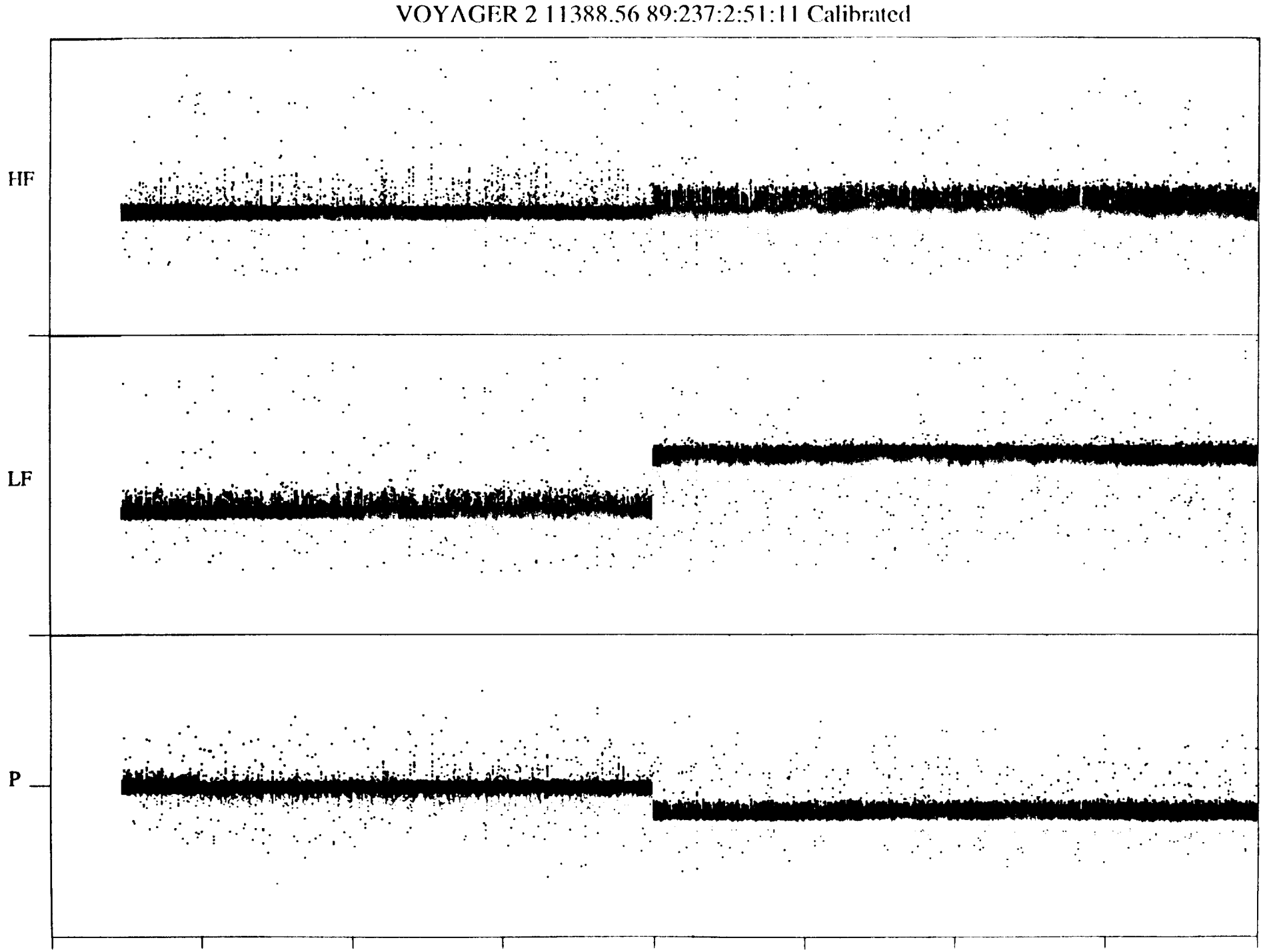

Figure 2

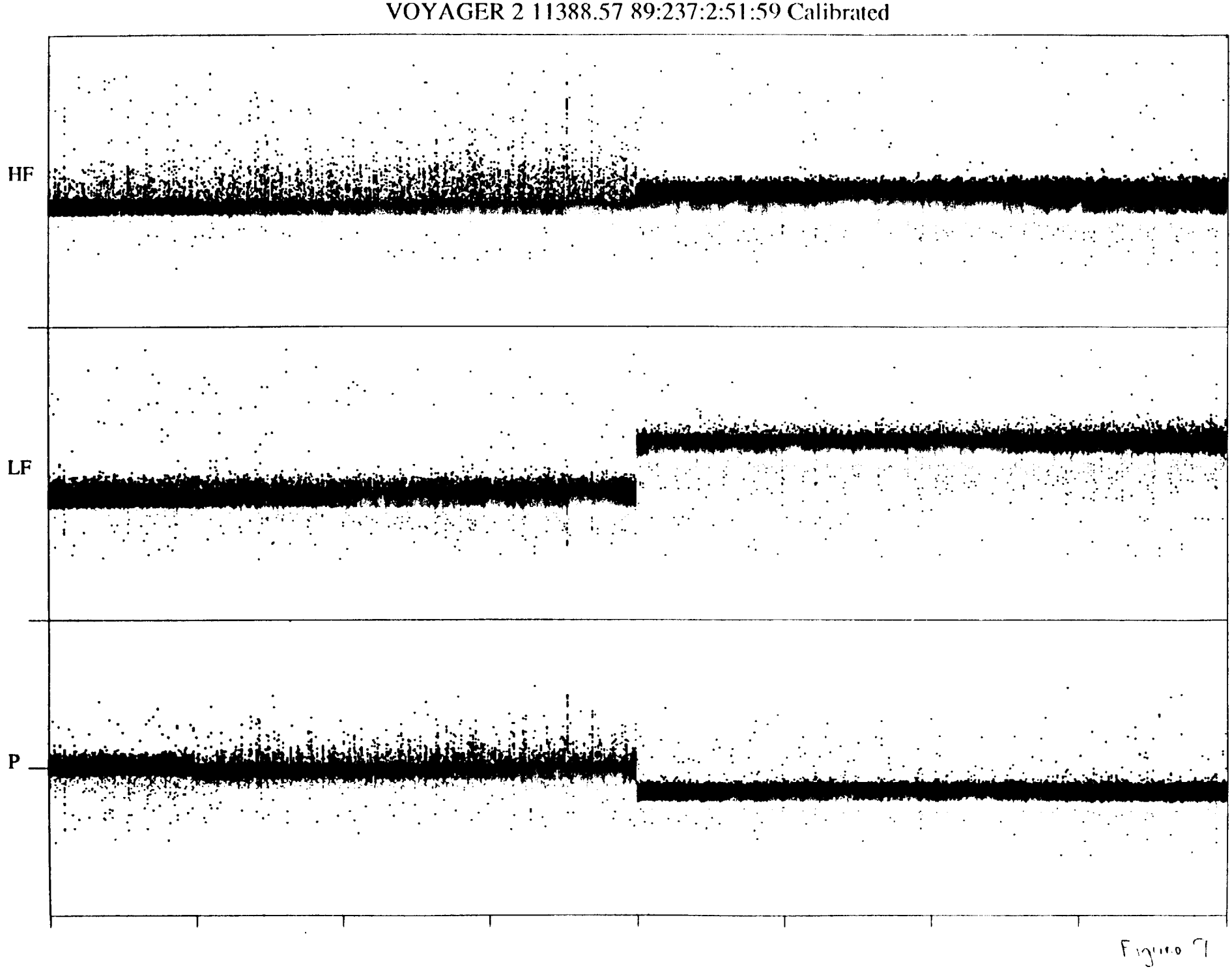

Figure 7

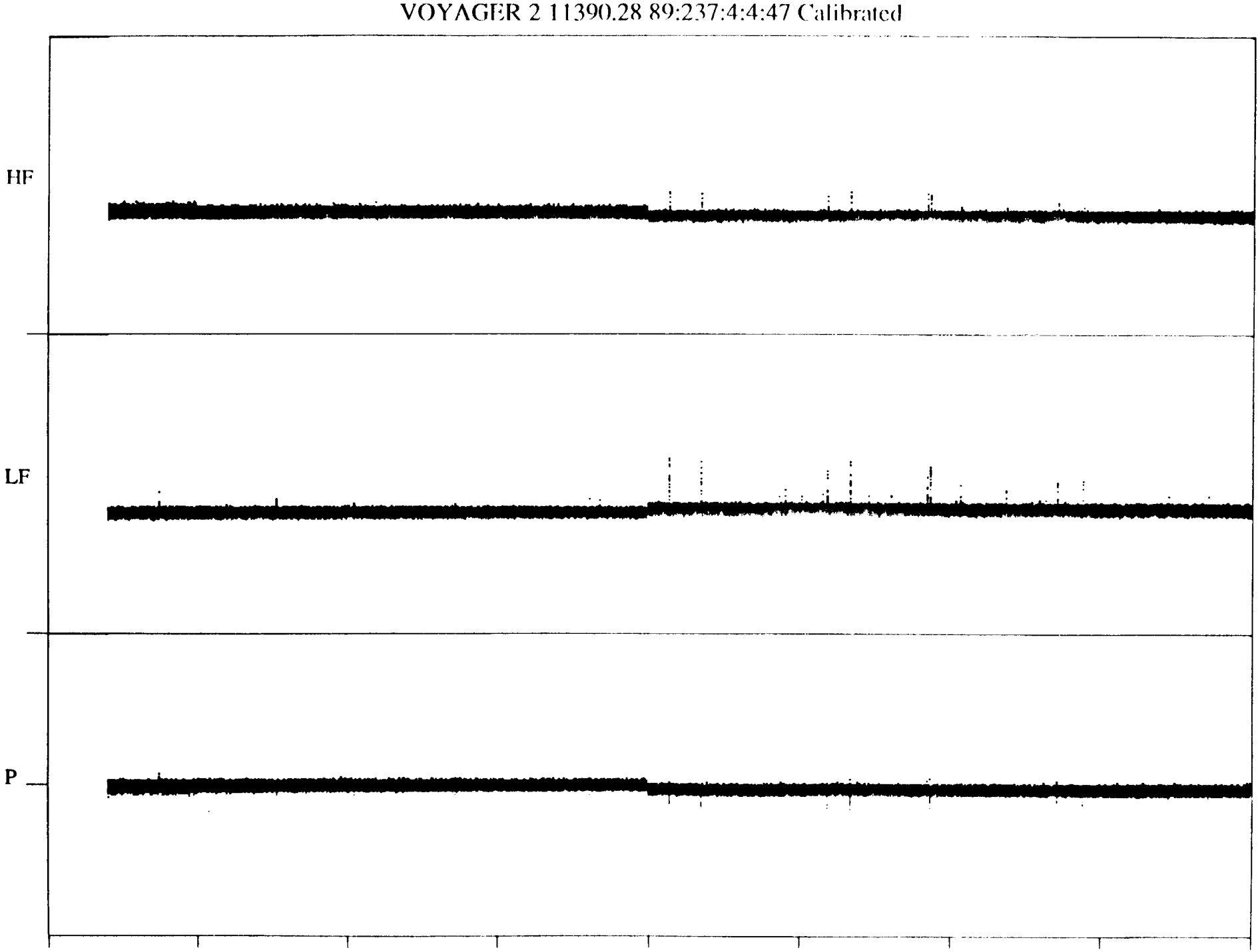

Figure 10

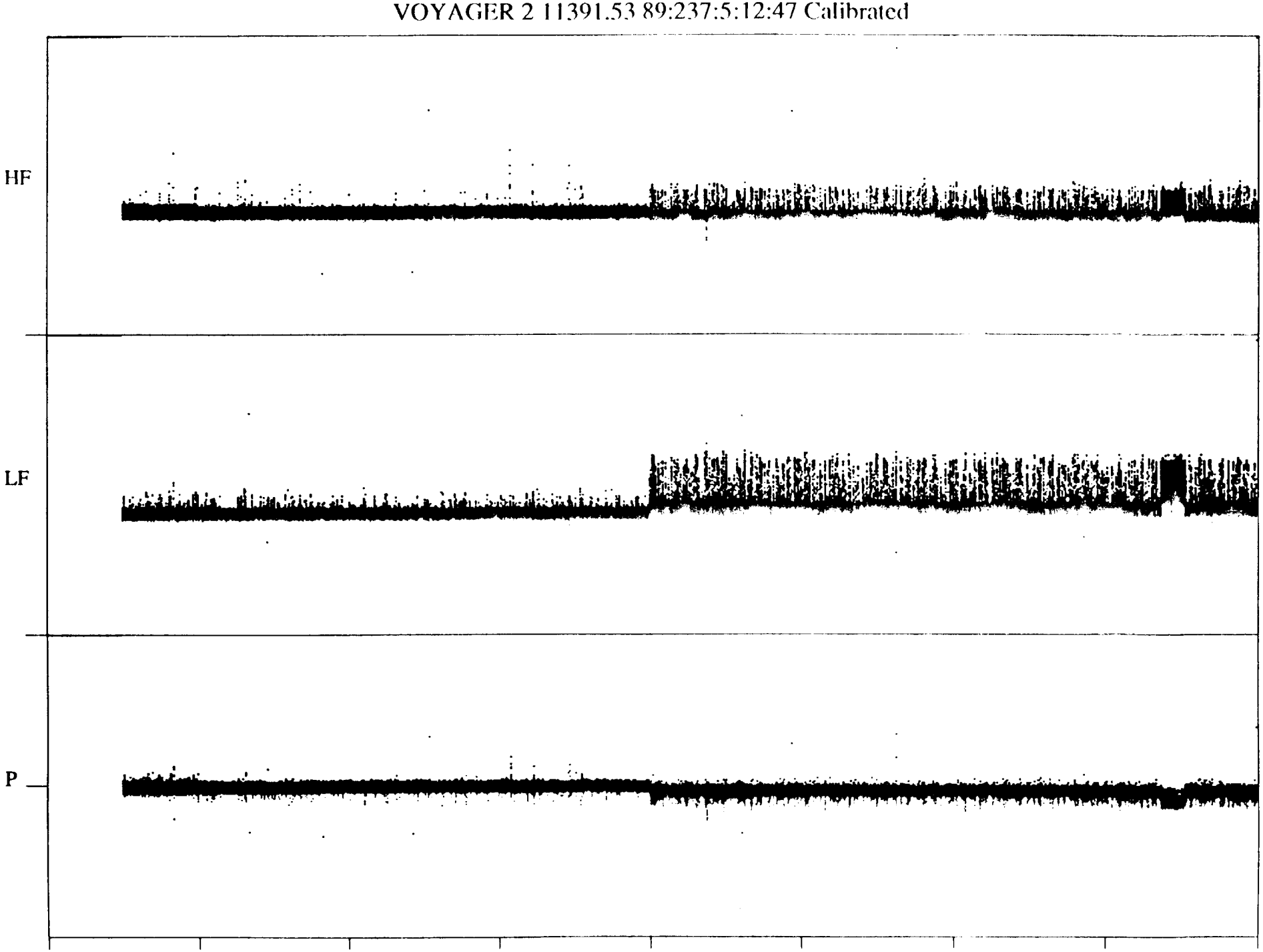

Figure 11

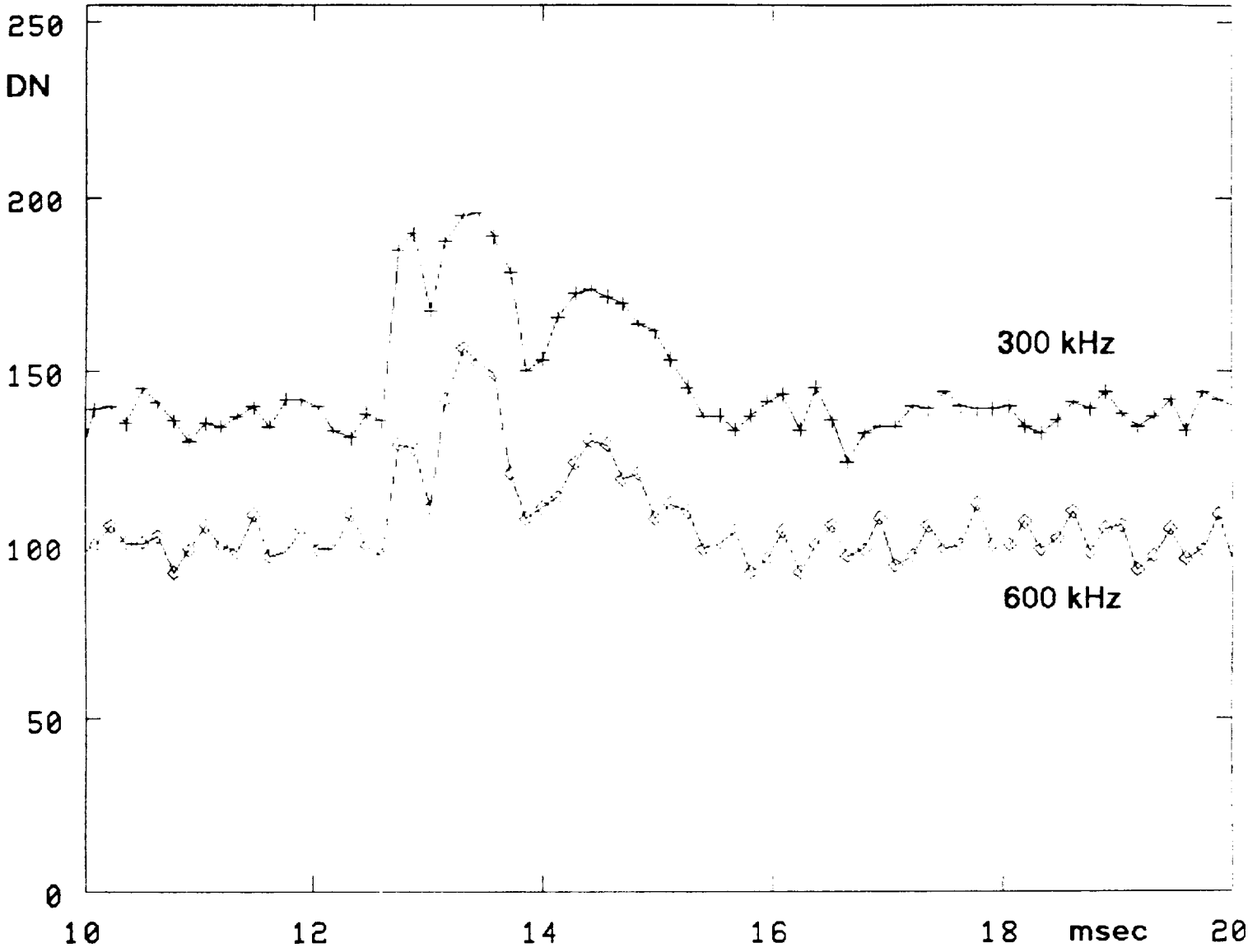

Figure 12

VOYAGER 2 89:237:2:47 GS-3

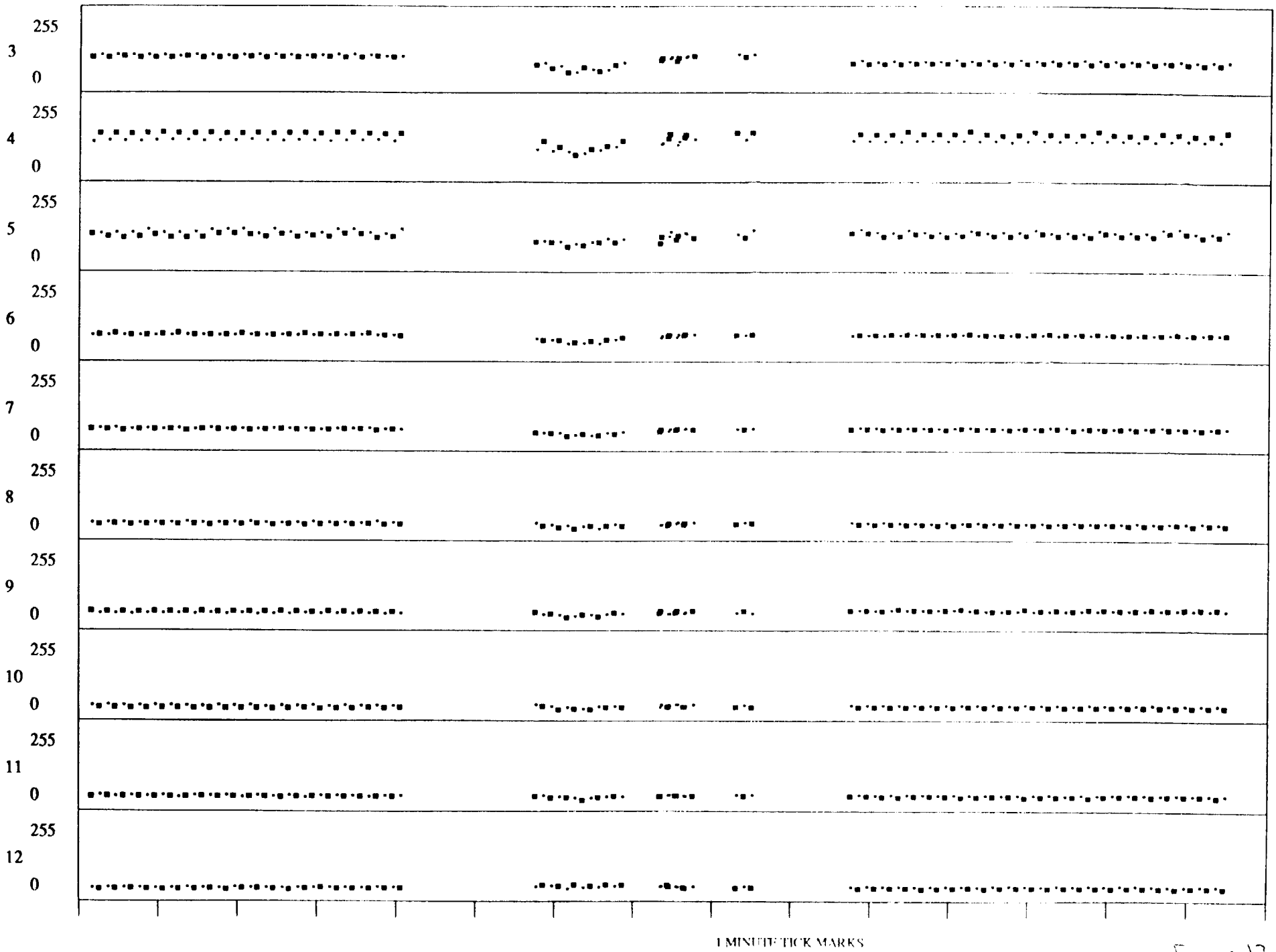

Figure 13

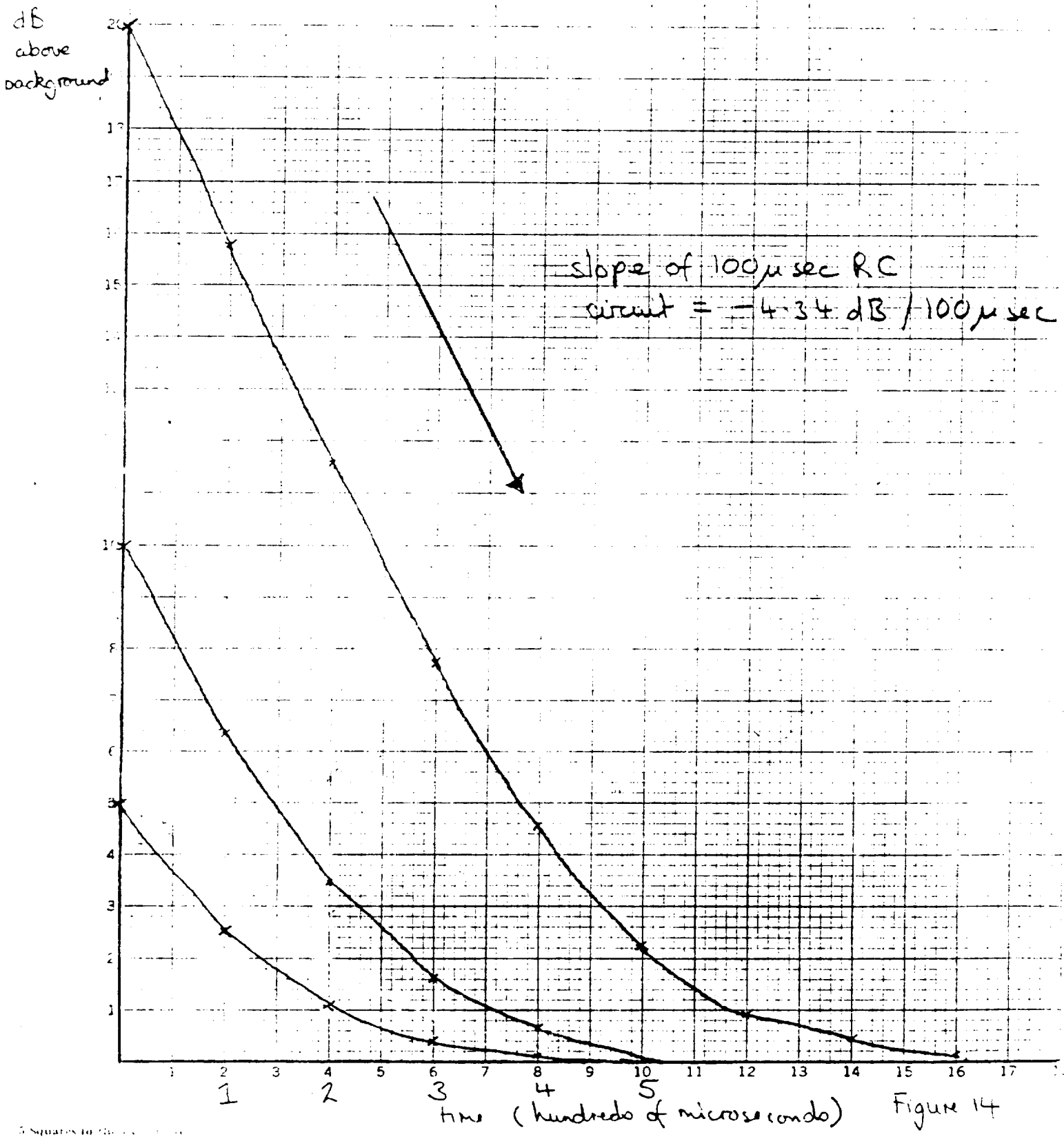
dB above background
slope of 100μsec RC circuit = −4.34 dB / 100μsec
time (hundreds of microseconds)

Figure 14

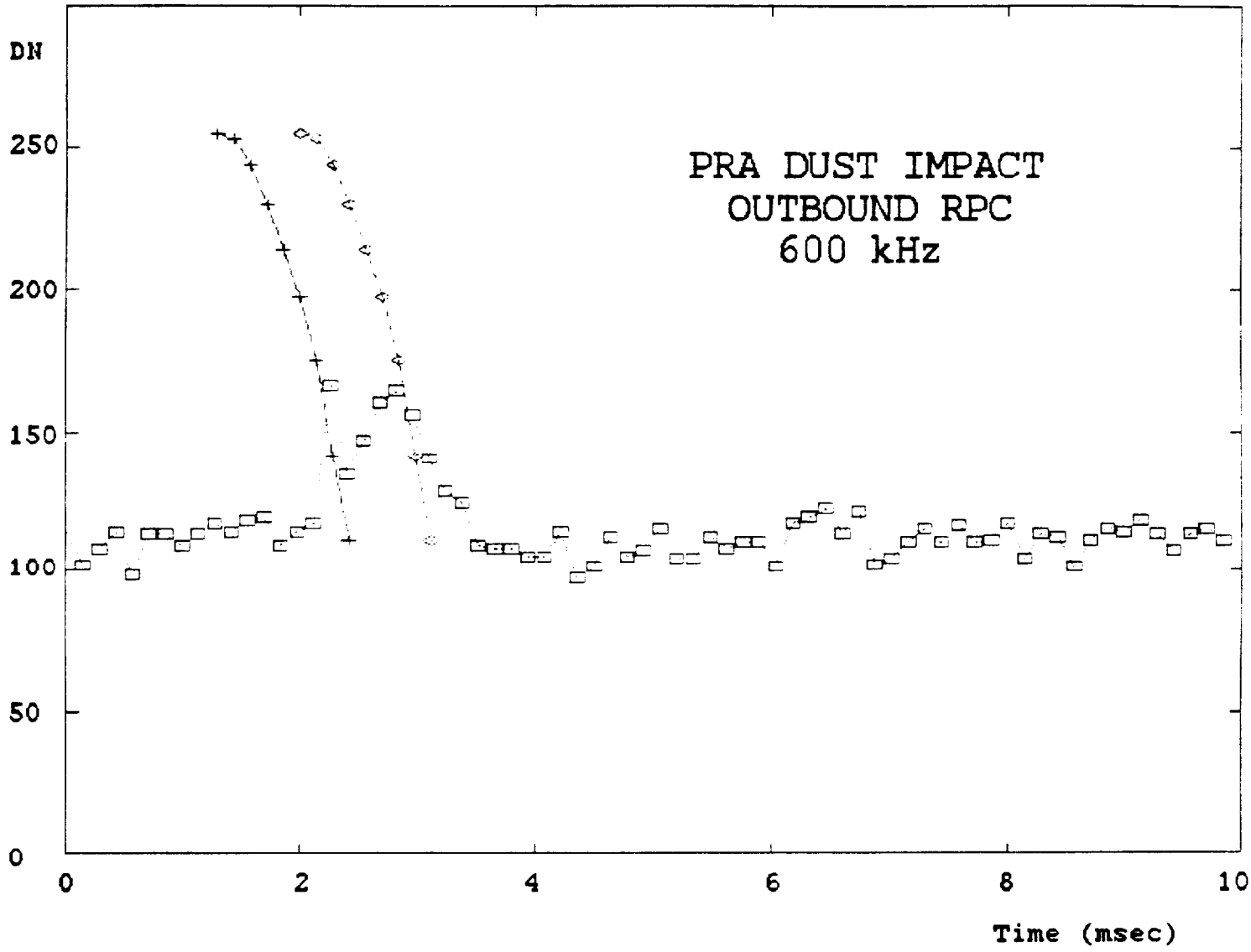
PRA DUST IMPACT
OUTBOUND RPC
600 kHz
DN
250
200
150
100
50
0
0
2
4
6
8
10
Time (msec)

Figure 15

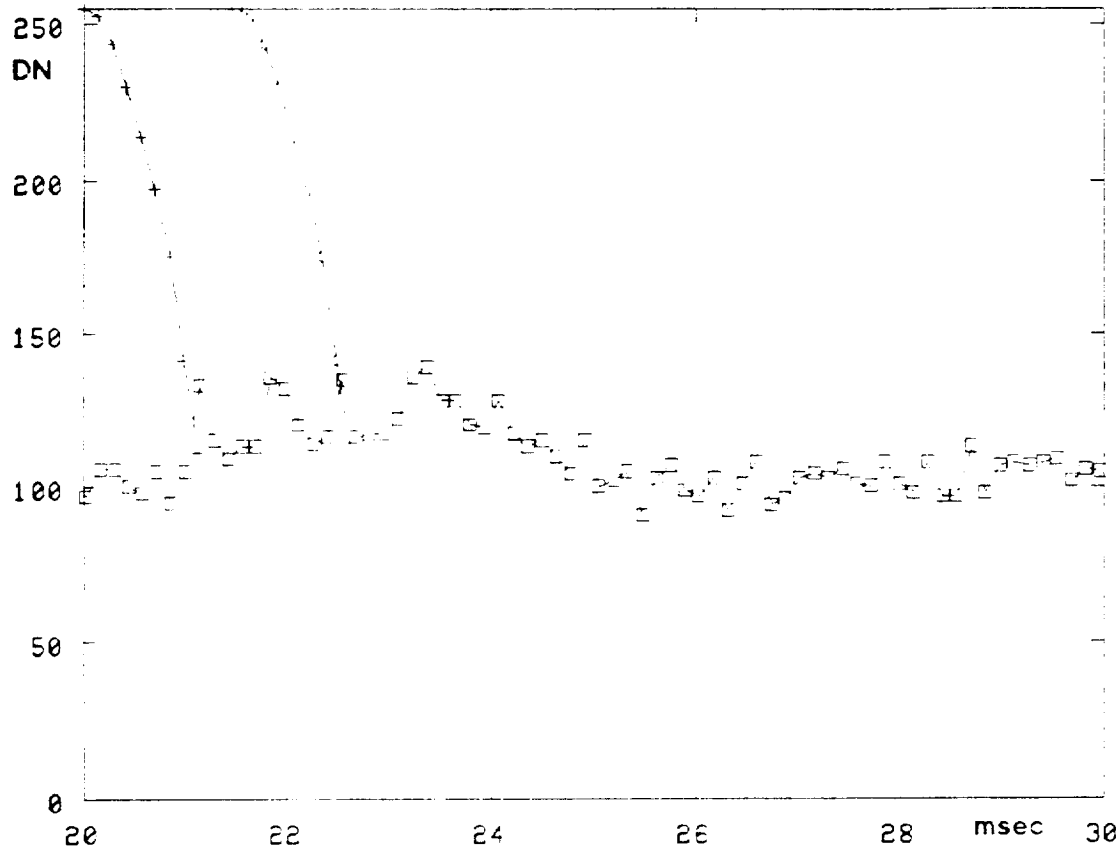
250
DN
200
150
100
50
0
20
22
24
26
28
msec
30

(a)

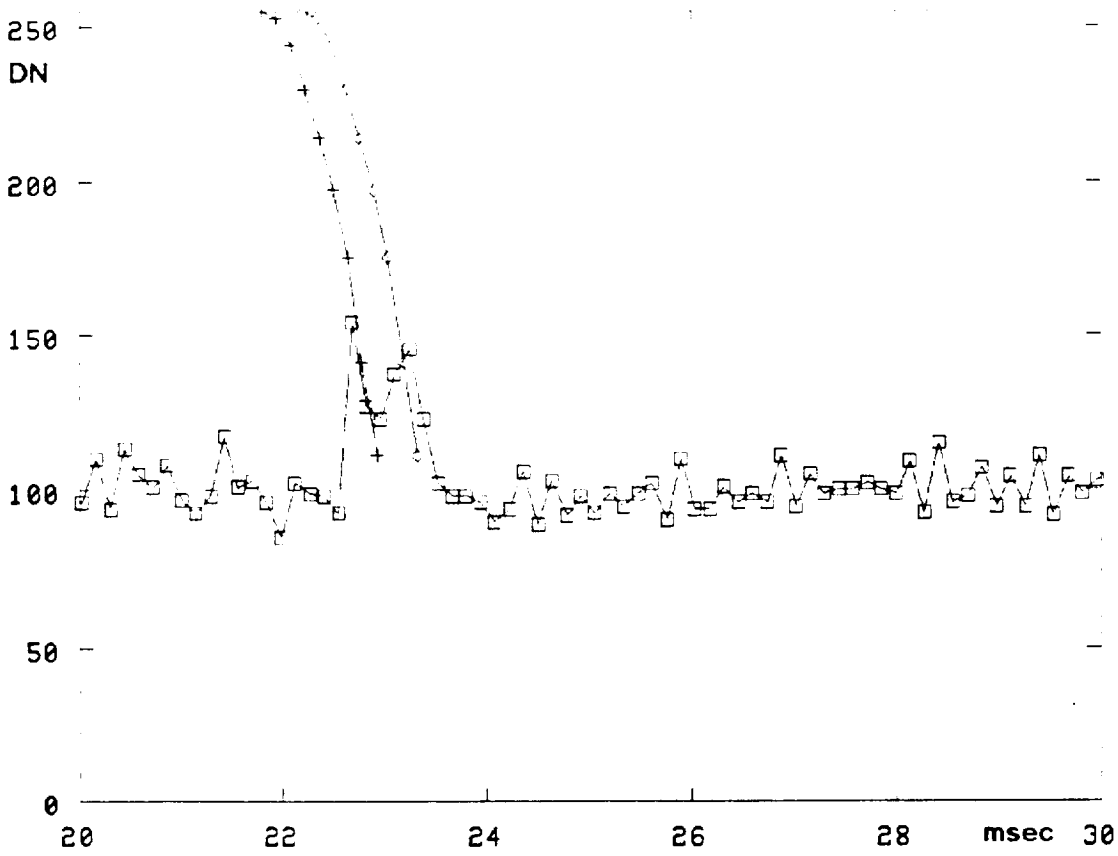
250
DN
200
150
100
50
0
20
22
24
26
28
msec
30

(b)

Figure 16

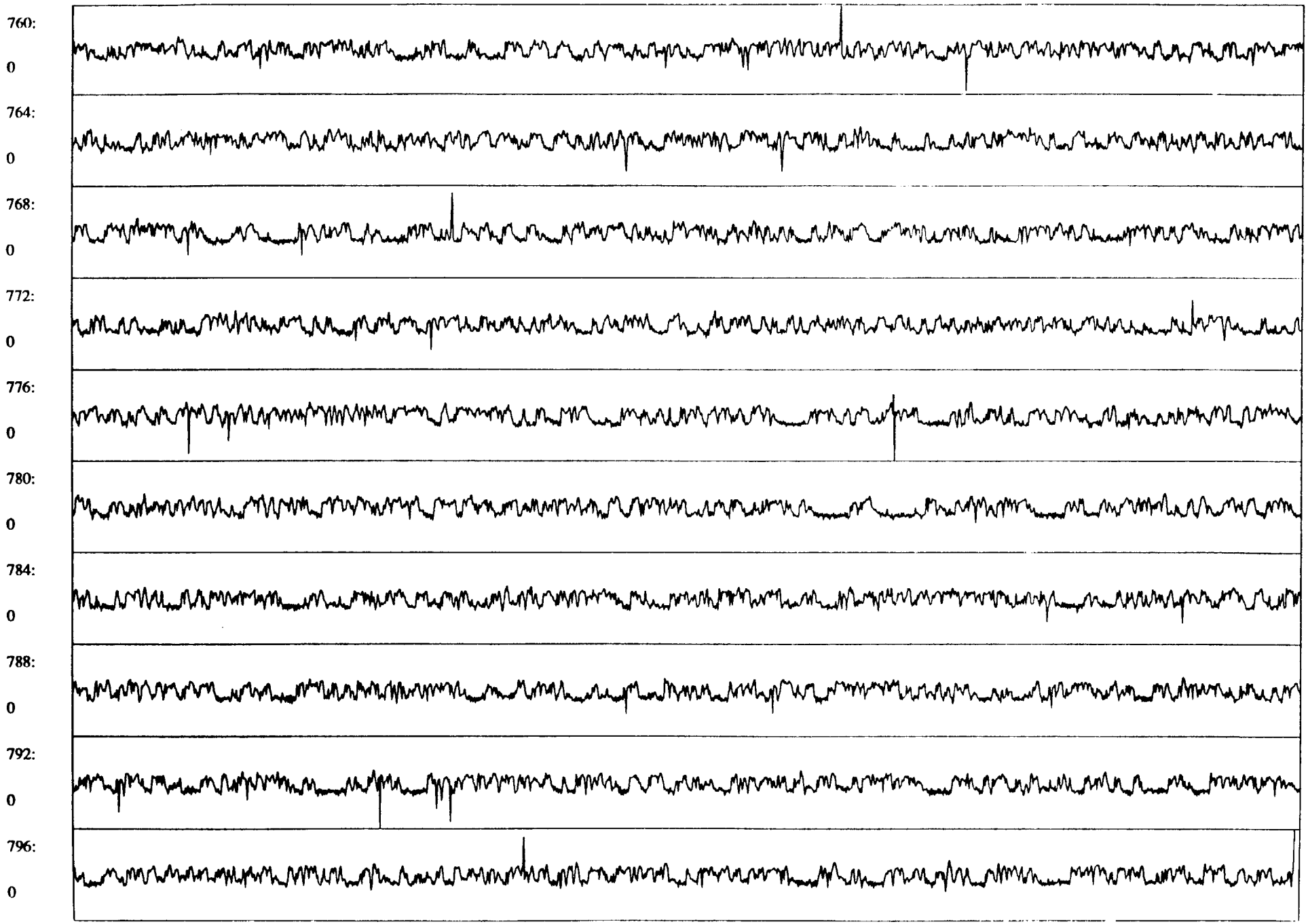
VOYAGER 2 11388.57 89:237:2:51:59 Ch2
760:
0
764:
0
768:
0
772:
0
776:
0
780:
0
784:
0
788:
0
792:
0
796:
0

Figure 17

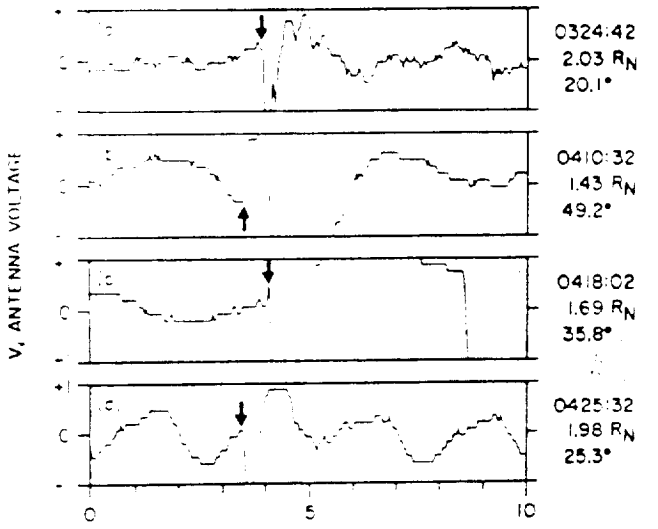
0324:42
2.03 R_N
20.1°
0410:32
1.43 R_N
49.2°
0418:02
1.69 R_N
35.8°
0425:32
1.98 R_N
25.3°
V, ANTENNA VOLTAGE
0
5
10
TIME (MILLISEC.)
VOYAGER 2, AUG. 25, 1989

Figure 5

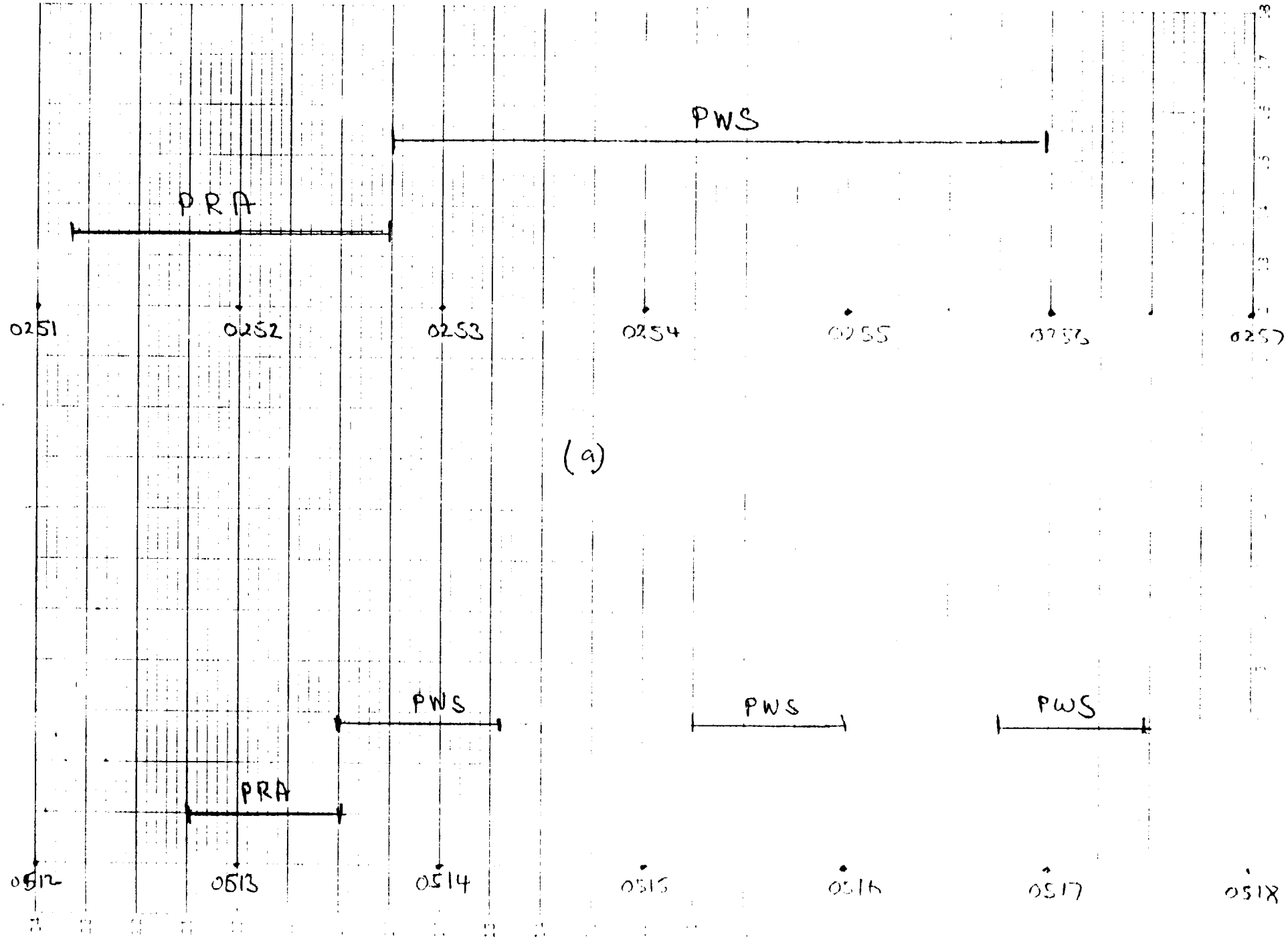
PWS
PRA
0251
0252
0253
0254
0255
0256
0257
(a)
PWS
PWS
PWS
PRA
0512
0513
0514
0515
0516
0517
0518
(b)

Figure 19

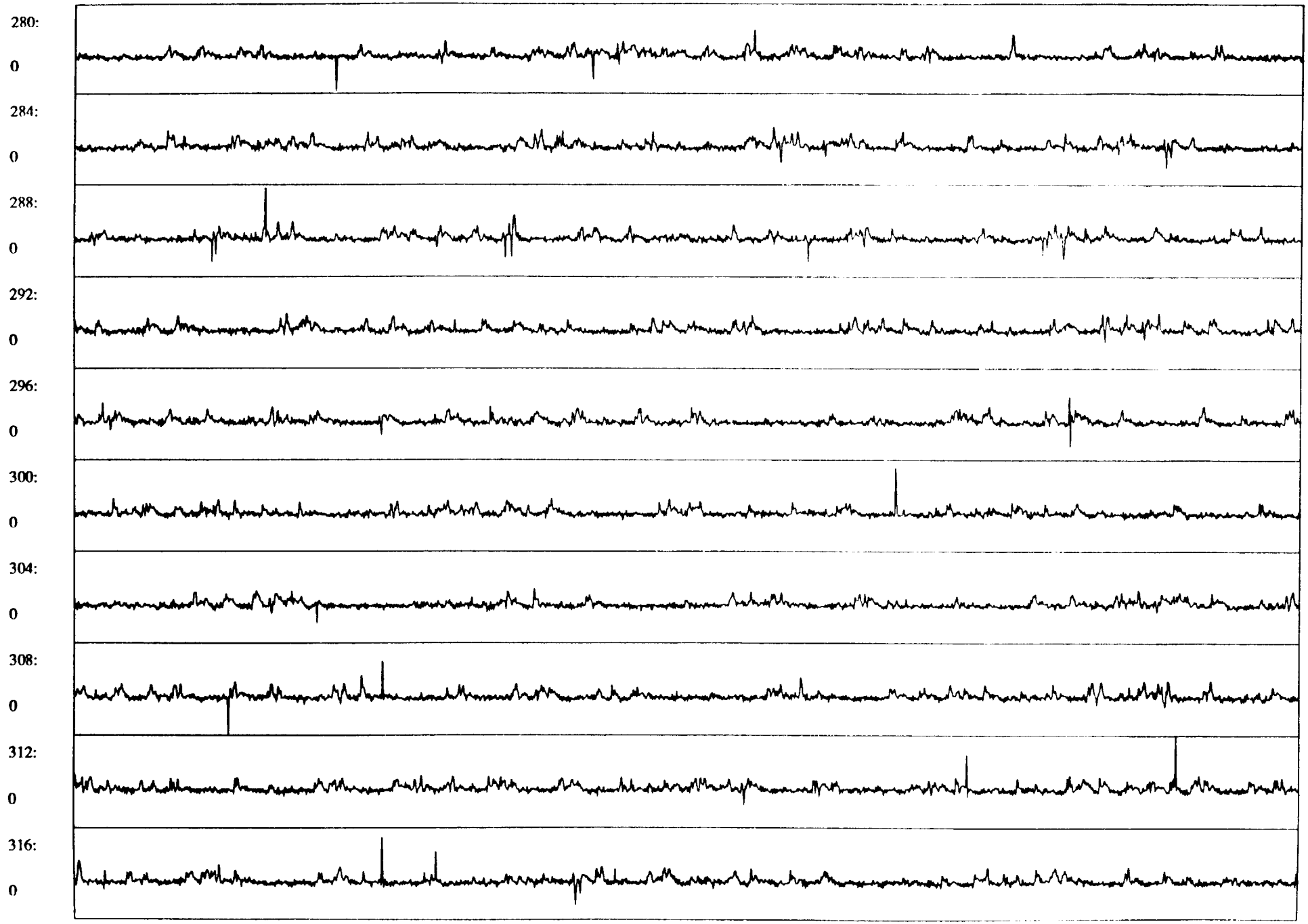
VOYAGER 2 11388.57 89:237:2:51:59 Ch1
280:
0
284:
0
288:
0
292:
0
296:
0
300:
0
304:
0
308:
0
312:
0
316:
0

Figure 20

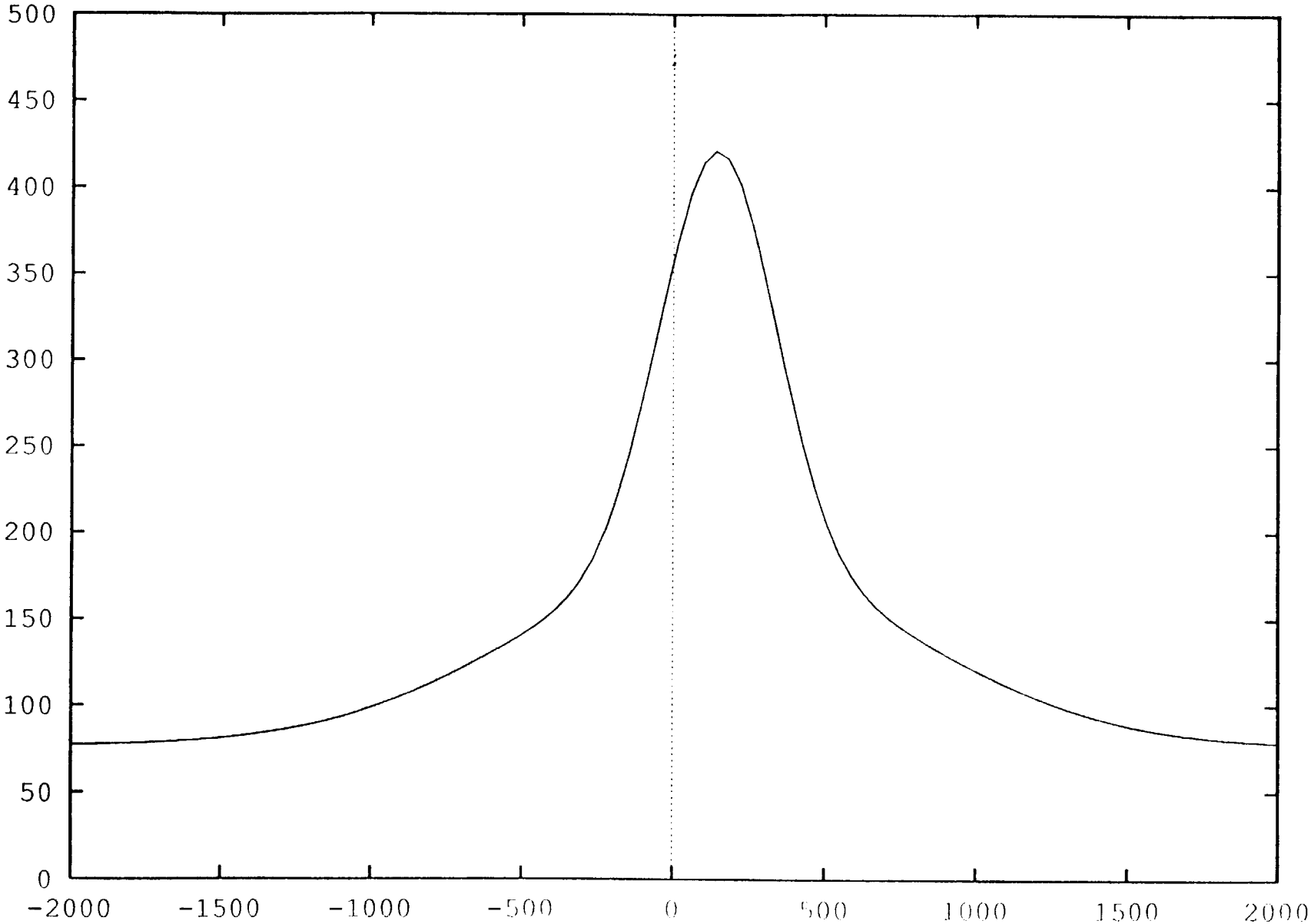
500
450
400
350
300
250
200
150
100
50
0
-2000
-1500
-1000
-500
0
500
1000
1500
2000

Figure 21

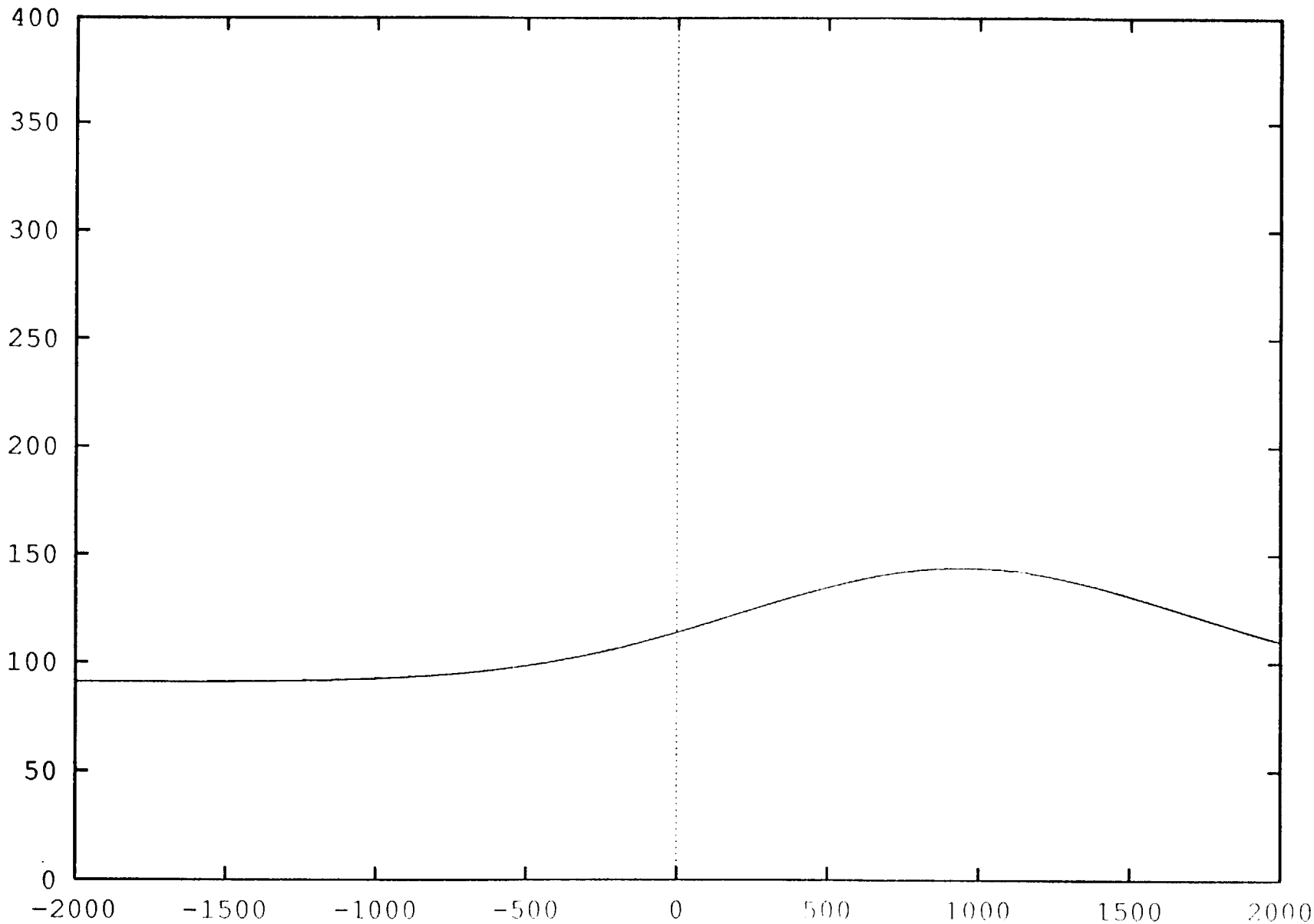
400
350
300
250
200
150
100
50
0
-2000
-1500
-1000
-500
0
500
1000
1500
2000

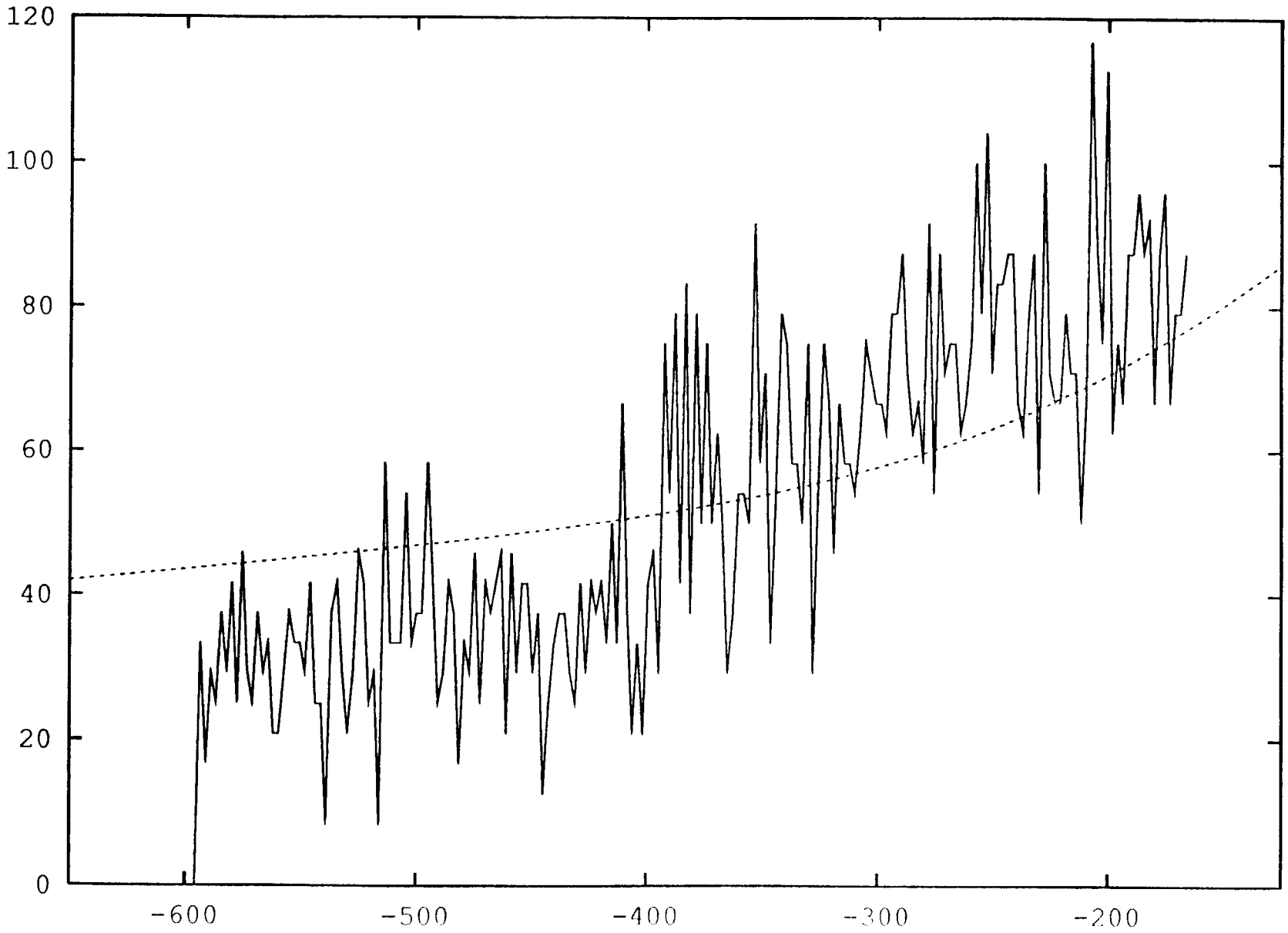

Figure 2.2

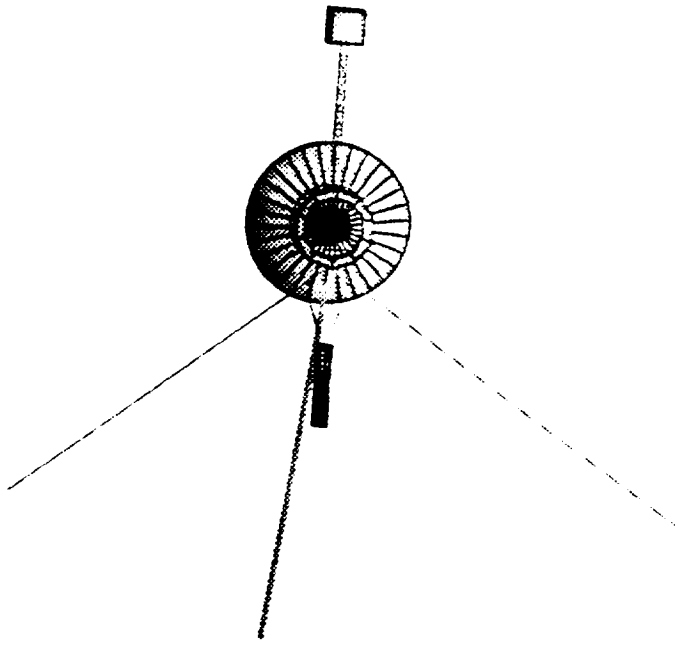

Figure 24

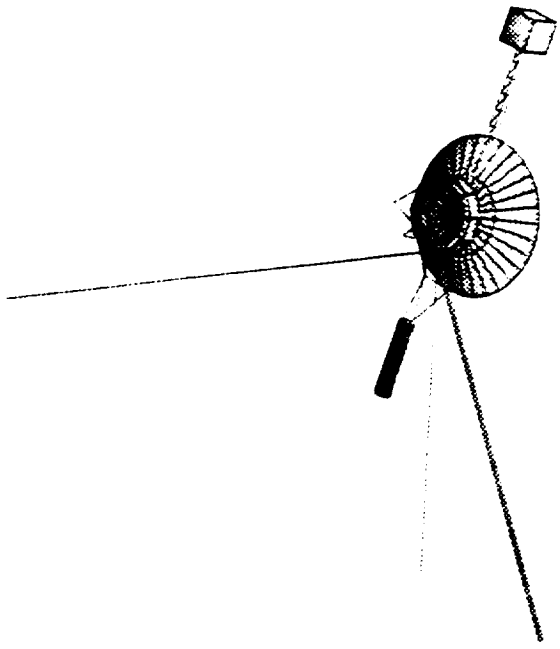

Figure 25

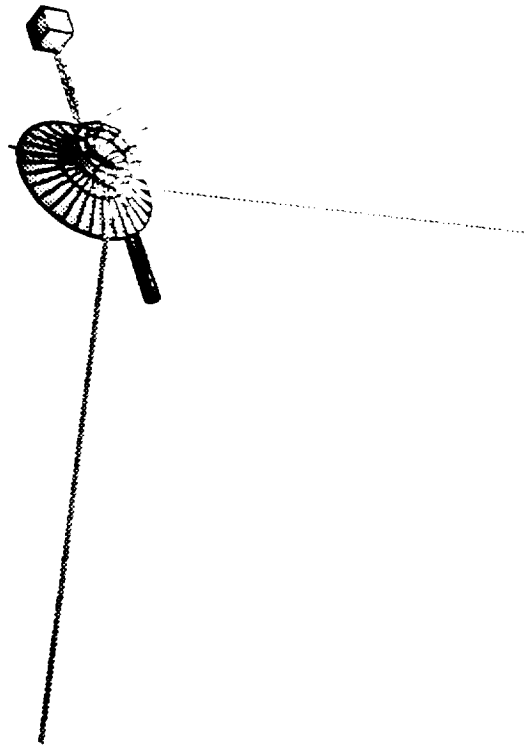

Figure 26

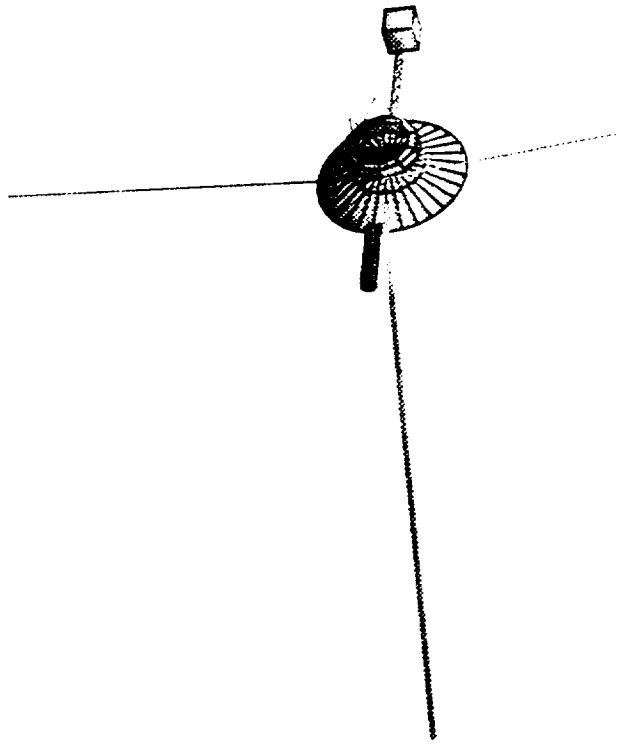

Figure 27

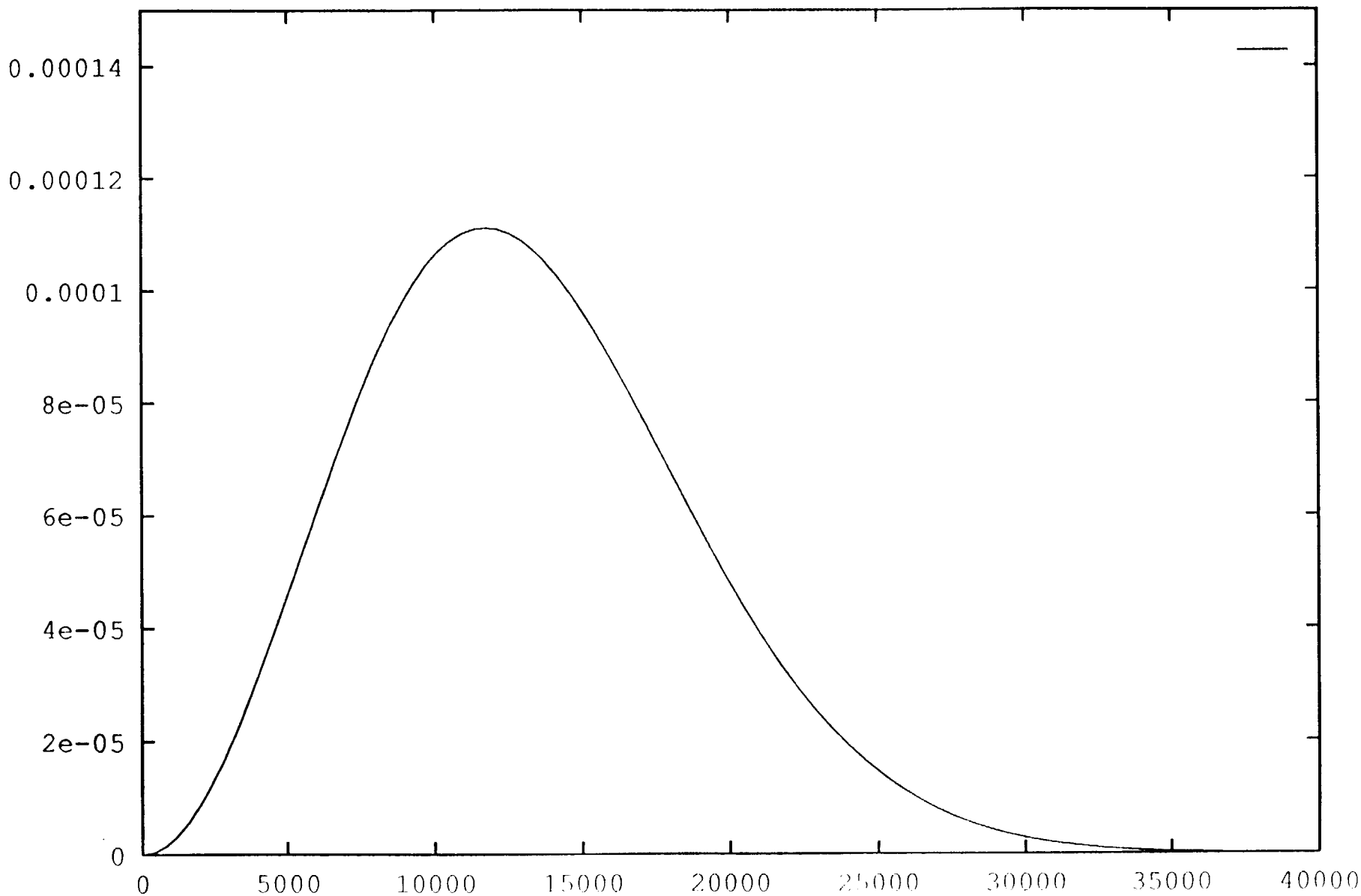
0.00014
0.00012
0.0001
8e-05
6e-05
4e-05
2e-05
0
0
5000
10000
15000
20000
25000
30000
35000
40000

Figure 28

REPORT DOCUMENTATION PAGE

Form Approved
OMB No. 0704-0188

1. AGENCY USE ONLY (Leave blank)	2. REPORT DATE	3. REPORT TYPE AND DATES COVERED
	July 13, 1993	5-14-91 -- 4-30-93

4. TITLE AND SUBTITLE
Detection of Dust Impacts by the Voyager Planetary Radio Astronomy Experiment

5. FUNDING NUMBERS
NASW-4617

6. AUTHOR(S)
David R. Evans

7. PERFORMING ORGANIZATION NAME(S) AND ADDRESS(ES)
Radiophysics, Inc.
5475 Western Avenue
Boulder, CO 80301

8. PERFORMING ORGANIZATION REPORT NUMBER

9. SPONSORING/MONITORING AGENCY NAME(S) AND ADDRESS(ES)
NASA Headquarters

10. SPONSORING/MONITORING AGENCY REPORT NUMBER

11. SUPPLEMENTARY NOTES

12a. DISTRIBUTION/AVAILABILITY STATEMENT

12b. DISTRIBUTION CODE

13. ABSTRACT (Maximum 200 words)
See attached

14. SUBJECT TERMS
Neptune, Dust Impacts, Voyager 2, Radio Astronomy

15. NUMBER OF PAGES
57

16. PRICE CODE

17. SECURITY CLASSIFICATION OF REPORT	18. SECURITY CLASSIFICATION OF THIS PAGE	19. SECURITY CLASSIFICATION OF ABSTRACT	20. LIMITATION OF ABSTRACT
Unclassified	Unclassified	Unclassified	UL

NSN 7540-01-280-5500

Standard Form 298 (Rev. 2-89)
Prescribed by ANSI Std. Z39-18
298-102

NASW-4617

ABSTRACT

The PRA instrument detected large numbers of dust particles during the Voyager 2 encounter with Neptune. We here analyse the signatures of these impacts in some detail. The major conclusions are:-

1. PRA detects impacts from all over the spacecraft body, not just the PRA antennas;

2. The signatures of individual impacts last substantially longer than was expected from complementary PWS data acquired by another Voyager experiment;

3. The signatures of individual impacts demonstrate very rapid fluctuatiions in signal strength, so fast that the data are limited by the speed of response of the instrument;

4. The PRA detects events at a rate consistently lower than does the Plasma Wave subsystem;

5. Even so, the impact rate is so great near the inbound crossing of the ring plane that no reliable estimate of impact rate can be made for this period;

6. The data are consistent with the presence of electrons accelerated by ions within an expanding plasma cloud from the point of impact.

An ancillary conclusion is that the anomalous appearance of data acquired at 900 kHz appears to be due to an error in processing the PRA data prior to their delivery to the experiment's Principal Investigator, rather than due to overload of the PRA instrument.